CMS Draft Analysis Note

The content of this note is intended for CMS internal use and distribution only

2012/06/28
Head Id: 40099
Archive Id: 121928M
Archive Date: 2011/02/18
Archive Tag: trunk

Search for Long-Lived Particles using Displaced Photons in pp Collisions at $\sqrt{s} = 7\,\text{TeV}$

Daniele Del Re, Shahram Rahatlou, Michael Sigamani, and Livia Soffi
INFN Sezione di Roma "La Sapienza", Rome, Italy

Abstract

We present the results of a search for long-lived particles decaying into photons in proton-proton collisions at a center-of-mass energy of 7 TeV by the CMS experiment at the LHC. We use the Missing Transverse Energy and the time of impact of the photon on the surface of the Electromagnetic Calorimeter to search for an excess of events over the Standard Model background expectation. After the final selection, using a data set of 4.86 ± 0.11 fb^{-1}, no significant excess is observed so we proceed to set limits on the production cross-section of $\widetilde{\chi}_1^0 \to \gamma\widetilde{G}$ at 95% C.L. and place a lower limit of 220 GeV/c^2 and 6000 mm respectively on the mass and $c\tau$ of the $\widetilde{\chi}_1^0$.

1 Introduction

The Standard Model (SM) of particle physics has proven extremely successful, but despite its many successes, still remains incomplete. Theoretical motivations provide compelling rationale for searches into long-lived particles decaying into final states with photons and Missing Transverse Energy ($\not{E}_{\mathrm{T}}$). We have seen that this is a clean, well-motivated, and powerful discovery channel for new physics. Of particular theoretical interest are supersymmetry (SUSY) models with gauge-mediated SUSY-breaking (GMSB) [1]. These models have been long been studied as candidates for new physics beyond the TeV energy scale, and coupled with the relatively high production cross section and striking experimental signature allow for discoveries using early LHC data. Many versions of these models employ a similar phenomenology, so we choose a benchmark scenario as our search model. This scenario is commonly described as 'Snowmass Slope and Parameter Set 8' (SPS8) [2]. In this scenario the neutralino ($\tilde{\chi}_1^0$) is the next-to-lightest supersymmetric particle and decays almost exclusively into a photon (γ) and a weakly interacting stable gravitino ($\tilde{G}$). The $\tilde{G}$ is the lightest supersymmetric particle (LSP), and gives rise to $\not{E}_{\mathrm{T}}$ by leaving the detector without depositing any energy, and is a promising dark matter candidate (theorised mass in the range $0.5 < m_{\tilde{G}} < 1.5$ keV$/c^2$). Furthermore, assuming R-parity conservation, we expect pairwise production of the $\tilde{\chi}_1^0$. We note that the most stringent limits using the benchmark GMSB model on the mass of the $\tilde{\chi}_1^0$ to are greater than 175 GeV$/\mathrm{c}^2$ [3–5].

We use the GMSB model to tune our studies but we want to remain sensitive to general searches for long-lived particles decaying into photons produced in association with jets, and not only R-parity conserving SUSY. Therefore event-by-event we search for single photons produced from a displaced vertex. Since the photon is produced from a displaced vertex it will be detected by the Electromagnetic Calorimeter (ECAL) later with respect prompt photons. In the case of no significant excess observed above the estimated SM background, we will set about setting an upper-limit on the Branching Fraction times cross-section of the $\tilde{\chi}_1^0 \to \tilde{G}\gamma$ decay. Therefore, important variables in this study are the ECAL timing, the cluster shape of the energy deposit in the ECAL and $\not{E}_{\mathrm{T}}$

The main SM backgrounds will arise from mis-identified photons and mis-measured $\not{E}_{\mathrm{T}}$. These include QCD events which can mimic the signature of $\tilde{\chi}_1^0 \to \tilde{G}\gamma$ decay due to the badly reconstructed photons and the presence of fake $\not{E}_{\mathrm{T}}$. Requirements on calorimeter and track isolation are used to reduce this contribution. Alongside the QCD background we also expect a contribution from γ+jet, which is an important background due to the presence of a real isolated photon, and fake $\not{E}_{\mathrm{T}}$ (from mis-reconstruction of photons) in the final state. Although the presence of a real, high P_T, isolated photon can mimic the signature of the signal, the event topology is very different between γ+jet and GMSB signal events. We expect that γ+jet events are characterised by a lower jet multiplicity with respect to our signal, and therefore a requirement on the minimum number of jets above a P_T threshold is expected to reject a large fraction of this background. For these backgrounds we estimate their contribution with data-driven control samples (CS). Alongside processes which give rise to fake $\not{E}_{\mathrm{T}}$, we also have a real $\not{E}_{\mathrm{T}}$ contribution from Electroweak (EWK) decays. These include $W \to e\nu$, where the lepton can fake the presence of a photon, and the ν giving rise to real $\not{E}_{\mathrm{T}}$ in the event. For the same reasons, we expect some contribution from $\mathrm{t\bar{t}}$ decays where the top quark decays almost 100% of the time into a W boson with a b quark. The W boson then decays to leptons which can produce a $\gamma+\not{E}_{\mathrm{T}}$ signature, with the $\not{E}_{\mathrm{T}}$ arising due to one or more neutrinos. To estimate the contribution of all the background apart from QCD and γ+jet we use Monte Carlo (MC) simulations normalised to the cross section provided by CMS. Alongside the backgrounds described above, we also expect some events which do not originate from proton-proton collisions. These backgrounds

include cosmic rays, beam-halo muons, and ECAL spikes. Since the ECAL time and $\not\!\!E_{\mathrm{T}}$ can be large for these events, they must be understood. We discuss the vetoes which we use in order to bring this contribution down to negligible levels.

2 Datasets and Trigger

2.1 Data

The data analysed corresponds to an integrated luminosity of 4.86 ± 0.11 fb^{-1}, collected and reconstructed using `CMSSW_4_2_3`. Only luminosity-sections certified as GOOD in the official good run file were used and the datasets analysed correspond to:

199.1 pb^{-1}: `/Photon/Run2011A_May10ReReco-v1/AOD`
951.1 pb^{-1}: `/Photon/Run2011A_PromptReco-v4/AOD`
352.4 pb^{-1}: `/Photon/Run2011A_05Aug2011-v1/AOD`
684.9 pb^{-1}: `/Photon/Run2011A_PromptReco-v6/AOD`
2670.0 pb^{-1}: `/Photon/Run201_PromptReco-v1/AOD`
JSON: `Cert_160404-180252_7TeVPromptReco_Collisions11_JSON.txt`

2.2 Background and signal Monte Carlo

The MC events used in this analysis are generated at centre of mass energy $\sqrt{s} = 7$ TeV using Summer 2011 prescriptions, and reconstructed using `CMSSW_4_2_3`. The MC is generated using PYTHIA [6] and MADGRAPH [7], and processed with a simulation of the CMS detector using the GEANT4 package [8]. For $\mathrm{t\bar{t}}$ + jets, W+jets, and Drell Yan +jets the secondary τ decays are handled by TAUOLA [9]. The QCD multi-jet and γ+jet MC datasets are generated in a wide $\hat{\mathrm{P}_T}$ range[1]. The event sample size for each $\hat{\mathrm{P}_T}$ bin, the cross section (σ) at the leading order (LO) and the equivalent integrated luminosity are listed in Table 1. For the GMSB signal, approximately 50,000 events per parameter-point were generated. The generation follows the SPS8 proposal, where the free parameters are the SUSY breaking scale (Λ), and the $\widetilde{\chi}_1^0$ flight-length ($c\tau_{\widetilde{\chi}_1^0}$) are varied to cover an appropriate range of phase space. These signal points are documented in Table 5 in the appendix along with their respective cross-sections. Furthermore, depending on the value of SUSY breaking scale, 4%–15% of the GMSB signal also decay as $\widetilde{\chi}_1^0 \rightarrow Z^0\widetilde{G}$, which can be seen in Table 6. In the case of the final limits, we are conservative and assume 100% branching fraction for the branching fraction of $\widetilde{\chi}_1^0 \rightarrow \gamma\widetilde{G}$. The masses for the $\widetilde{\chi}_1^0$ are proportional to Λ and are calculated using the SUSYHIT package [10].

2.3 Trigger

The primary triggers used for our search are `Photon75_CaloIdVL_IsoL` (runs 160410-165120), `Photon90_CaloIdVL_IsoL` (runs 165121-178421), and `Photon90EBOnly*IsoL_TriPFJet25` (178421-180252). All of which are seeded using `L1_SingleEG20`. The first two triggers have an online requirement of $\sigma_{i\eta i\eta} < 0.024$, ECAL Iso/$E_t(\gamma) < 0.2$, HCAL Iso (isolation)/$E_t(\gamma) < 0.2$, and $H/E < 0.15$ and P_T greater than 75 and 90 GeV respectively. The final trigger has additional requirements of $\eta < 1.4$ and three or more Particle-Flow (PF) [11] jets above 25 GeV/c. All offline selection cuts are chosen to be tighter than the HLT selection, and we see from Figure 1 that both triggers become 100% efficient with an offline cut of $\mathrm{P}_T(\gamma) > 100\,\mathrm{GeV}$ (see Figure 28 left), and $\mathrm{P}_T^{\mathrm{jet}} > 35\,\mathrm{GeV}$.

[1] where $\hat{\mathrm{P}_T}$ is the transverse momentum of one of the two partons in the rest frame of the hard process

Process	Kinematic cut [GeV]	σ_{LO} [pb]	No. events	$\mathcal{L}$ [pb]$^{-1}$
QCD	$50 < \hat{P_T} < 80$	6.4×10^6	2.0×10^5	3.0×10^{-2}
QCD	$80 < \hat{P_T} < 120$	7.8×10^5	3.7×10^6	4.7×10^1
QCD	$120 < \hat{P_T} < 170$	1.1×10^5	5.7×10^6	5.2×10^1
QCD	$170 < \hat{P_T} < 300$	2.4×10^4	6.2×10^6	2.6×10^2
QCD	$300 < \hat{P_T} < 470$	1.1×10^3	5.7×10^6	5.2×10^3
QCD	$470 < \hat{P_T} < 600$	7.0×10	3.3×10^6	4.7×10^4
QCD	$600 < \hat{P_T} < 800$	1.5×10	2.7×10^6	1.8×10^5
QCD	$800 < \hat{P_T} < 1000$	1.8	8.0×10^5	1.7×10^6
γ+jet	$50 < \hat{P_T} < 80$	2.7×10^3	2.0×10^6	2.7×10^2
γ+jet	$80 < \hat{P_T} < 120$	4.5×10^2	1.9×10^6	4.2×10^3
γ+jet	$120 < \hat{P_T} < 170$	8.4×10^1	2.0×10^6	2.4×10^4
γ+jet	$170 < \hat{P_T} < 300$	2.3×10^1	2.0×10^6	8.7×10^4
γ+jet	$300 < \hat{P_T} < 470$	1.5	1.7×10^6	1.1×10^6
γ+jet	$470 < \hat{P_T} < 800$	1.3×10^{-1}	2.1×10^6	1.6×10^7
γ+jet	$1400 < \hat{P_T} < 1800$	1.3×10^{-5}	2.2×10^6	2.1×10^{11}
$t\bar{t}$ + jet	-	9.5×10	3.6×10^6	3.8×10^4
V+γ+jet	-	5.7×10^1	1.2×10^6	2.1×10^4
W+jets	-	2.8×10^4	6.5×10^6	2.3×10^2
Drell Yan +jets	-	2.5×10^4	5.6×10^6	2.2×10^4

Table 1: The description of the background MC samples used in this analysis

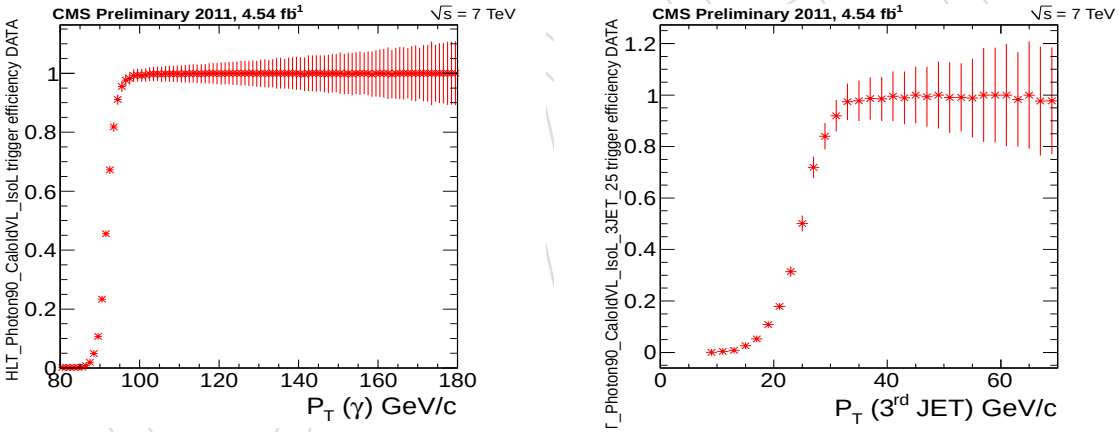

Figure 1: The trigger efficiency turn-on using the photon pT for `Photon90_CaloIdVL_IsoL` (left) and jet pT for `Photon90EBOnly_CaloIdVL_IsoL_TriPFJet25` (right)

3 Reconstruction and Event Selection

The event selection for this analysis requires at least one high P_T isolated photon with at least three jets in the final state. The selection on the jets is based on a 2010 optimisation study to minimise the expected upper limit. The study was the repeated using 2011 pile-up (PU) conditions and similar results were attained.

3.1 Cluster shape

One of the distinctive features of an off-pointing photon is the shape of the energy deposit it leaves in the ECAL (see Figure 2). The shower shape has been previously used to discriminate energy deposits from photons and neutral pions [12].

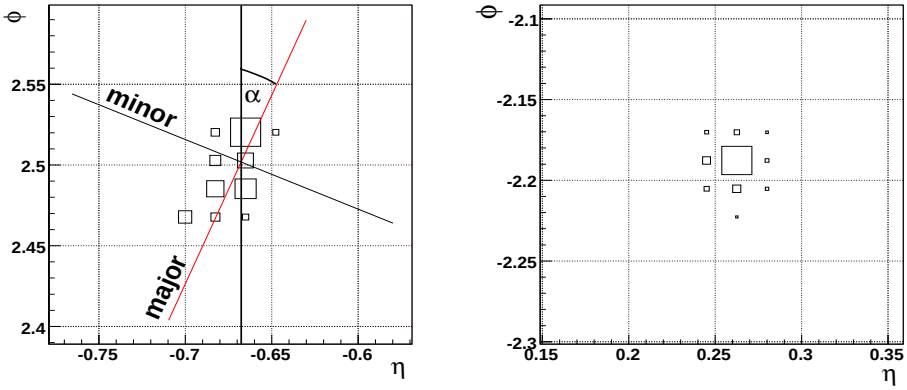

Figure 2: The Energy distribution in the ECAL crystals for a non-pointing (left) and pointing (right) photon

This variable is computed using the geometrical properties of the energy deposit in the ECAL, and can be described using the following covariance matrix:

$$\mathrm{COV}_{\eta\phi} = \begin{pmatrix} S_{\eta\eta} & S_{\eta\phi} \\ S_{\phi\eta} & S_{\phi\phi} \end{pmatrix} \tag{1}$$

with,

$$S_{\mu\nu} = \sum_{i=1}^{N} w_i \left(\mu_i - \langle\mu\rangle\right)\left(\nu_i - \langle\nu\rangle\right) \tag{2}$$

where N is number of crystals in the cluster, μ_i and ν_i are the η, ϕ indices respectively for i-th crystal of the cluster, and $\langle\mu\rangle = \frac{\sum_i w_i \cdot \mu_i}{\sum_i w_i}$. The logarithmic weight w_i, defined as:

$$w_i = \max\left[4.2 + \log\left(\frac{E_i}{E_{CLUSTER}}\right); 0\right] \tag{3}$$

The covariance matrix can be diagonalised in order to find the major and minor axes of the ellipse from the energy deposit. So

$$\mathrm{COV}_{\eta\phi} = \begin{pmatrix} \mathrm{S}_{Major} & 0 \\ 0 & \mathrm{S}_{Minor} \end{pmatrix} \tag{4}$$

with

$$\mathrm{S}_{\frac{Major}{Minor}} = \frac{S_{\phi\phi} + S_{\eta\eta} \pm \sqrt{\left(S_{\phi\phi} - S_{\eta\eta}\right)^2 + 4S_{\phi\eta}^2}}{2} \tag{5}$$

3.2 Pile-up

In order to account for pile-up (PU) we re-weight our MC following the recommended re-weighting schemes outlined in [13, 14]. The distribution of the number of vertices after re-weighting can be seen in Figure 3 (left). Also, in Figure 3 (right) we see that the S_{major} distri-

111 butions overlaid for different values of the number of primary vertices does not change sig-
112 nificantly. From Figure 4 we see that the GMSB signal selection efficiency remains flat with
113 increased PU, with the isolation variables showing an efficiency of above 90% up to 20 primary
114 vertices.

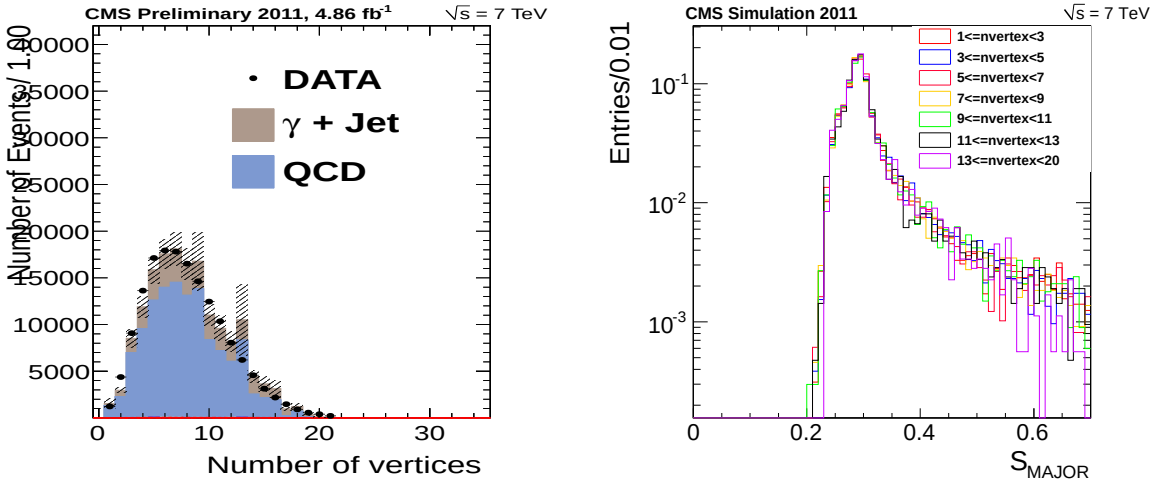

Figure 3: The distribution of the number of vertices after PU re-weighting (left), and the S_{Minor} (left) and S_{Major} (right) distributions overlaid for different values of number of primary vertices for the GMSB signal ($\Lambda = 100\,\text{GeV}$, $c\tau = 250\text{mm}$)

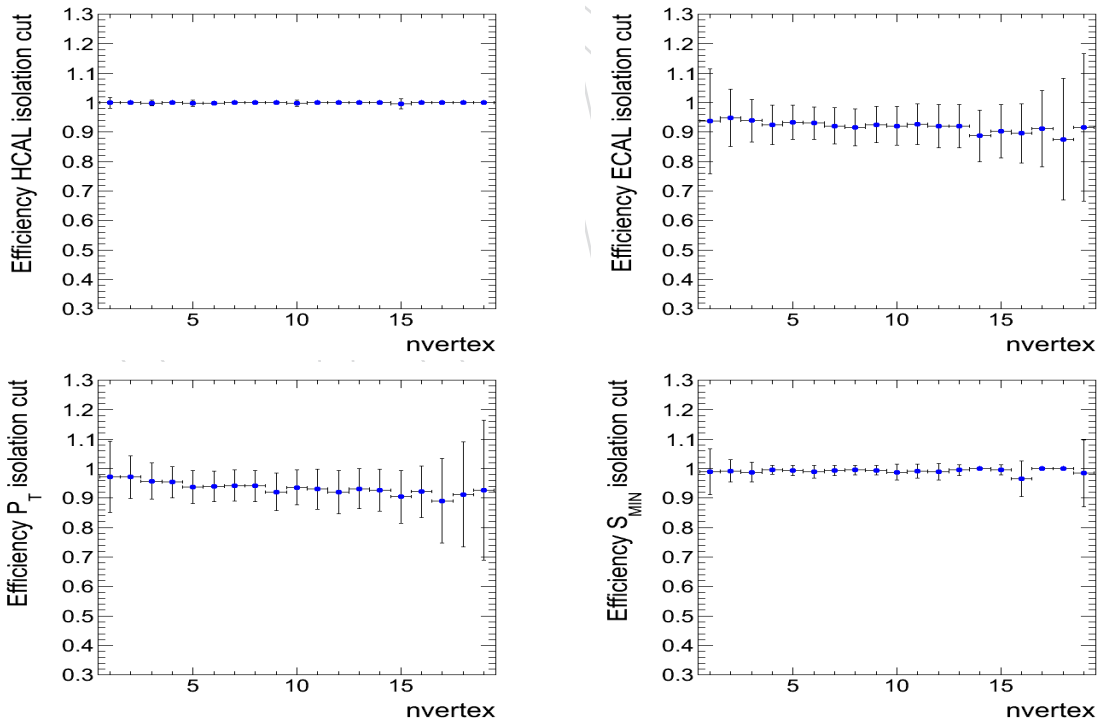

Figure 4: The HCAL Iso (top left), ECAL Iso (top right), S_{Minor} (bottom left), and TRK Iso (bottom right) cut efficiency for the GMSB signal ($\Lambda = 100\,\text{GeV}$, $c\tau = 250\text{mm}$) plotted against the number of primary vertices.

3.3 Pre-selection

We make use of a pre-selection which is defined as follows:

- $P_T(\gamma) > 70\,\text{GeV}$;
- (HCAL Iso/$P_T(\gamma) + \frac{H}{E}$) $\times$ E(γ) < 6.0;
- $0.1 < S_{Minor} < 0.53$;
- Good Vertex (vndof ≥ 4, $d_0 < 2$, $|z| < 24$).

From Table 9 we see that the `Photon` dataset is reduced to around 5% of its original value.

3.4 Photon reconstruction

The photon reconstruction begins with the identification of energy deposits in the ECAL according to dedicated supercluster algorithms which are discussed in detail in [15]. Standard CMS event cleaning requires a timing cut which is set as the number of sigma the channel is allowed to be out of time. The cut window is set at around 5σ, where σ is the resolution of the ECAL timing. The resolution at 1 GeV is less than 1 ns, and above 1 GeV flattens out. So this roughly translates into an event-by-event cut of ± 3 ns. It is also worth noting that this timing cut is double-sided (on the positive side) for gain 12. For gain 6 and gain 1, the upper cut is released. In order to retrieve the ECAL timing information we reconstruct our photon candidates using the 'uncleanHybridSuperClusters' collection stored in AOD. This operation returns us the original photon collection with the same energy, momentum, cluster shape and isolation variables available (we note however that the PixelVeto is not available).

In order to select good photon candidates we require HCAL, ECAL, and tracking isolation (hollow cone ΔR =0.4) for our photon candidates. We also place absolute thresholds as well as relative thresholds on the HCAL and ECAL isolation cuts in order to prevent requirements which are tighter than the noise level of the calorimeters. These isolation requirements are shown to be very efficient in rejecting QCD events, and also very efficient at selecting QCD events (discussed in our background estimation section). Furthermore, we find that $t\bar{t}$ events are heavily suppressed by tracking isolation. However, we see that γ+jet events are not easily rejected using isolation cuts due to the presence of a real isolated photon. So in order to reduce this contribution, we veto events where the leading jet back to back to photon, and

- $\Delta R(\gamma, jet) > 2/3$, where $\Delta R = \sqrt{(\phi_\gamma - \phi_{jet})^2 + (\eta_\gamma - \eta_{jet})^2}$;
- and $0.6 < p_T^{jet} / p_T^{\gamma} < 1.4$.

Also, we use the S_{Minor} variable to identify energy deposits in the ECAL compatible with isolated photons. In order to reject ECAL spikes we apply the standard PF topological cuts ($E6/E2 > 0.04$ and $E4/E1 > (0.04 * log(E1) - 0.024)$. To reject 'scraping' events produced by the interaction of beam-related protons with the LHC collimators, the fraction of tracks classified as high purity must exceed 20%. To reject events consistent with anomalous HCAL noise not due to instrumentation issues, we follow the recommendations from the HCAL Detector Performance Group (DPG) [16]. The PixelVeto requirement is not available due to the fact that we reconstruct our photons from the unclean supercluster collection in AOD. So in order to veto EWK events we reject GSF electrons found within a ΔR cone of 0.25 of the photon candidate. We also veto photons found in Trigger Tower 32 of Super-Module -16, which is known to have unreliable timing measurements. We reduce a large fraction of non-beam events by requiring a primary vertex in the pre-selection, with at least four associated tracks (vndof), whose position (d_0) is less than 2 cm from the centre of CMS in the direction transverse to the

beam and 24 cm in the direction along the beam ($|z|$) in each event. For beam-halo we use the CSC tight halo-cleaning outlined in [17]. Overall, from Figure 5-7 we see a good agreement between data and MC for all of the selection variables used in this analysis. For these Figures GMSB (2000) relates to $\Lambda = 100\,\text{GeV}$, $c\tau = 2000$ mm. And GMSB (250) relates to $\Lambda = 100\,\text{GeV}$, $c\tau = 250$ mm.

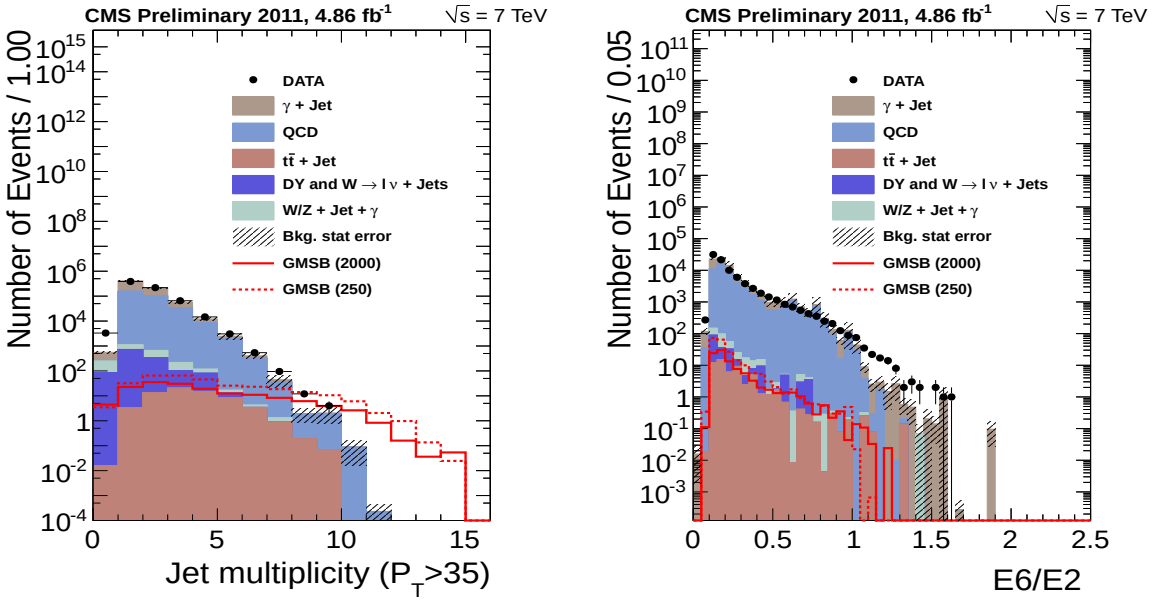

Figure 5: The distribution of the number of reconstructed jets with $P_T > 35$ GeV (left) and $E6/E2$ (right) with at least 3 jets above $P_T > 35$ for data and MC normalized to the luminosity of data after photon ID.

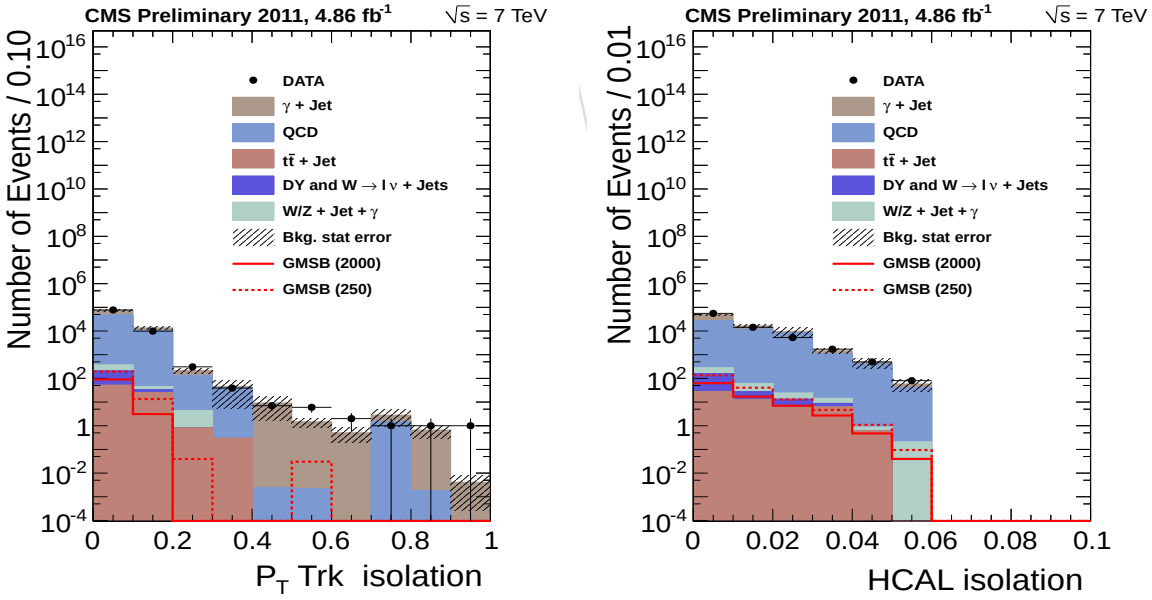

Figure 6: The distribution of $\sum P_T/P_T\,(\gamma)$ (left) and $\sum P_T$ (right) with at least 3 jets above $P_T >$ 35 (right) for data and MC normalised to the luminosity of data after photon ID.

The selection requirements for our final photon selection are listed as 'tight' in Table 2. The 'loose' will be discussed later, and is used for our QCD data-driven CS estimation. The isola-

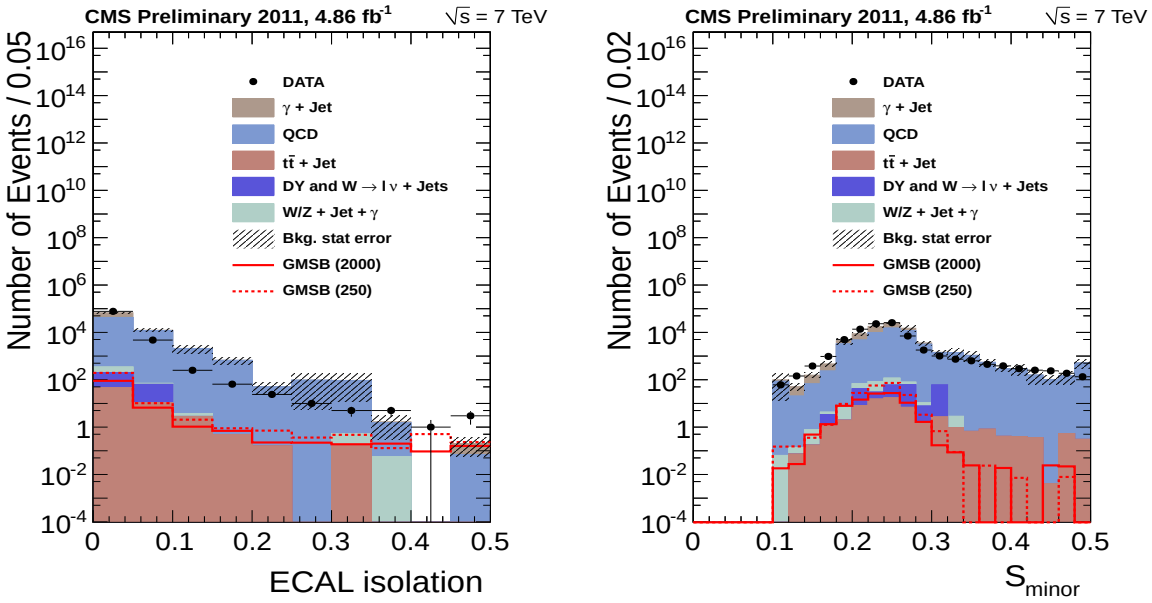

Figure 7: The distribution of $\sum$ECAL/E (γ) (left) and S_{Minor} (right) with at least 3 jets above $P_T > 35$ for data and MC normalised to the luminosity of data after photon ID.

tion criteria differs slightly from the recipe described by the `EGamma` group, where the motivation can be found in [18] which focuses on using cluster shape variable in displaced photon searches. The selection efficiencies can be seen in Tables 8, 9, and 10.

Criteria	Requirement (tight)	Requirement (loose)
$\lvert\eta\rvert$	< 1.4	< 1.4
$P_T(\gamma)$	> 100 GeV	> 100 GeV
Halo Veto	CSC Tight	CSC Tight
S_{Minor}	$0.15 < S_{Minor} < 0.3$	$0.15 < S_{Minor} < 0.7$
Electrons	Not associated to electron	Not associated to electron
Topological	E6/E2 and swiss-cross	E6/E2 and swiss-cross
ECAL time	> -2.0 ns	> -2.0 ns
HCAL Iso	$\sum$HCAL/E $(\gamma) < 0.05$ and $\sum$HCAL < 2.4 GeV	$\sum$HCAL/E $(\gamma) < 0.5$ and $\sum$HCAL < 6 GeV
ECAL Iso	$\sum$ECAL/E $(\gamma) < 0.05$ and $\sum$ECAL < 2.4 GeV	$\sum$ECAL/E $(\gamma) < 0.45$ and $\sum$ECAL < 5 GeV
TRK Iso	$\sum P_T/P_T(\gamma) < 0.1$	$\sum P_T/P_T(\gamma) < 0.45$

Table 2: The loose and tight photon ID selection criteria

3.5 Jet reconstruction

We use the number of jets above a P_T threshold as discriminating variable between GMSB signal and background, where a P_T threshold on the jet can allow for rejection of jets which do not originate from the fragmentation of prompt quarks. We reconstructed our jets using PF with anti-kt 5 [19] algorithm. We require jets with $P_T > 35$ GeV/c, and to be non-overlapping to photons ($\Delta R(\gamma, jet) > 0.5$) to avoid double counting with photons. Clean-up for PF Jets was studied using the procedure outlined in [20], requiring energy fractions on PF jets for neutral and charged hadrons. Any disagreement between data and MC arises due to calorimeter noise, spikes, and beam-related backgrounds. Side-band cuts are then applied in the regions of dis-

agreement improving the overall agreement between data and MC. In Figure 23 (appendix) we see a good overall agreement between data and MC therefore we conclude that jet cleaning of this kind will not be of benefit in this analysis. We require at least three jets in the final state, which removes close to 100% of beam-halo and cosmic events. As mentioned before, the selection on jets is based on a 2010 optimisation study to minimise the expected upper limit, which was also repeated using 2011 pile-up (PU) conditions with similar results were attained.

3.6 ECAL timing and $\not\!\!E_T$ calculation

The ECAL time is an important variable in identifying delayed photons for large regions of the signal parameter space where the $\tilde{\chi}_1^0$. This is also the case for the $\not\!\!E_T$, as used in most SUSY analyses. Therefore, we use these two variables in order to discriminate signal from background. We see from Figure 8 that the $\not\!\!E_T$ does not change significantly for different values of the $\tilde{\chi}_1^0$ lifetime therefore we assume a negligible correlation between these variables.

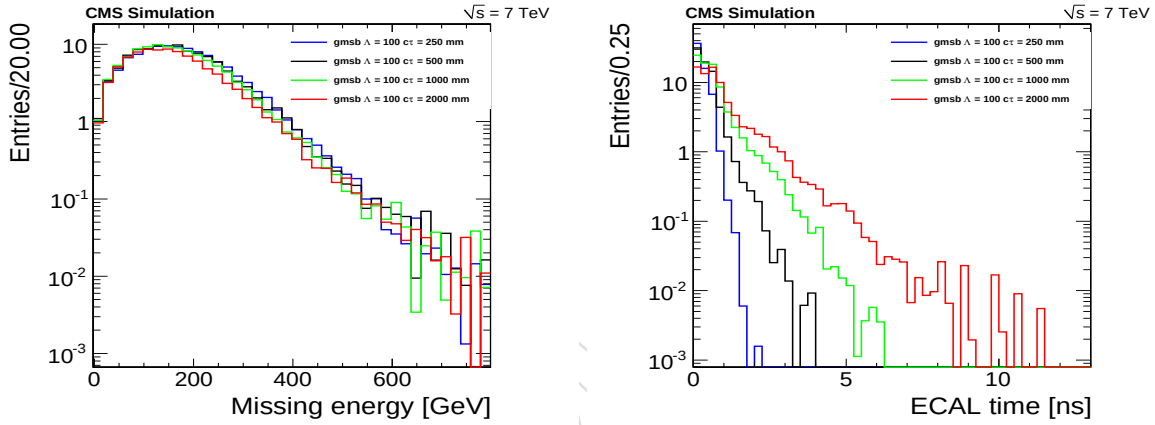

Figure 8: The distribution of the $\not\!\!E_T$ and ECAL time for different GMSB signal points

The $\not\!\!E_T$ is computed by summing the transverse momentum sum of all the particles in the event and is reconstructed using the PF algorithm. The ECAL time is computed using the weighted time of impact of all the RecHits within the supercluster associated to our signal photon. Due to mis-calibration effects an offset from zero is seen in the time distribution for both data and MC. In order to correct for this, and to reduce the error due to the uncertainty due to knowledge of the beam-spot position we pedestal the ECAL time measurement using an event-by-event correction. We start with a general definition for the ECAL time

$$\mathrm{T} = \frac{\Sigma \frac{T_i}{\sigma_i^2}}{\Sigma \frac{1}{\sigma_i^2}}, \tag{6}$$

where i are the RecHits used the calculation (above 1 GeV), and σ_i is the energy dependent uncertainty on the time measurement outlined in [21]. Concerning the ECAL time calculation for signal photons (T_{sig}), i, are the RecHits belonging to the signal photon supercluster. For the mean time of the event (T_{mean}), i, are all the RecHits in the event which do not belong to the two most energetic photons. So using the corrected timing T_{corr} defined as

$$T_{corr} = T_{sig} - T_{mean}, \tag{7}$$

and the uncertainty

$$\sigma_{T_{corr}} = \sqrt{\sigma^2_{T_{sig}} + \sigma^2_{T_{mean}}} \simeq \sigma_{T_{mean}} \tag{8}$$

we improve the resolution of the ECAL timing removing much of the dependance due the intrinsic jitter. We also correct for the offset in both data and MC using T_{corr}. To study if a dependance exists in terms of the mean and resolution of T_{corr} we perform a gaussian fit (Figure 9) as a function of η and the photon energy. The results of these studies can be seen in Figures 19–22 in the appendix. We see from Figure 10 (right) from the blue points that we observe an offset as a function of the photon energy. We account for this by vetoing the most energetic RecHit in the T_{corr} calculation if it has an energy above the first gain switch threshold (130 GeV).

Furthermore, in Figure 10 we see that the maximum deviation from zero is below 0.1 ns. We therefore use this as a conservative estimate for the event-by-event uncertainty due to the knowledge of the ECAL timing. Lastly, in order to correct for the difference in resolution seen between data and MC we apply a smearing to the ECAL time distribution in MC to match what we observe in data.

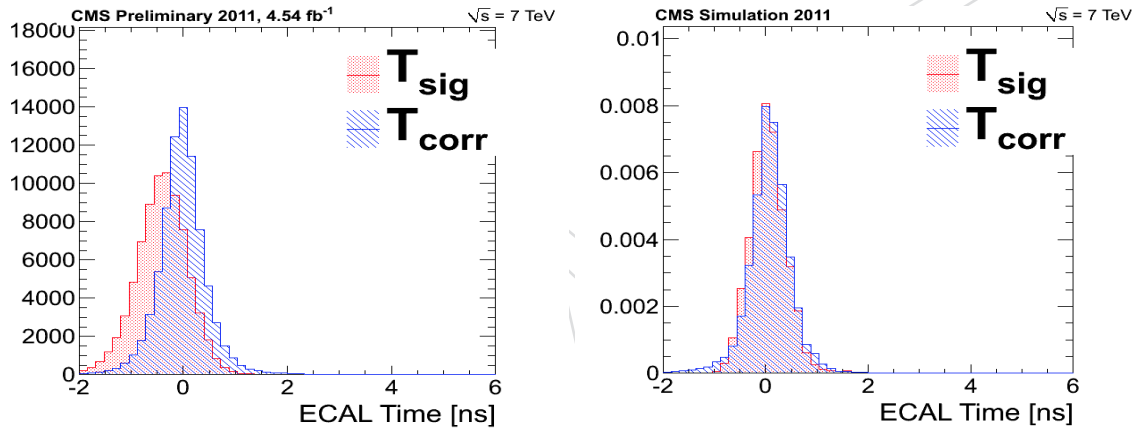

Figure 9: The ECAL time distribution for data (left) and MC (right) before and after the mean time correction

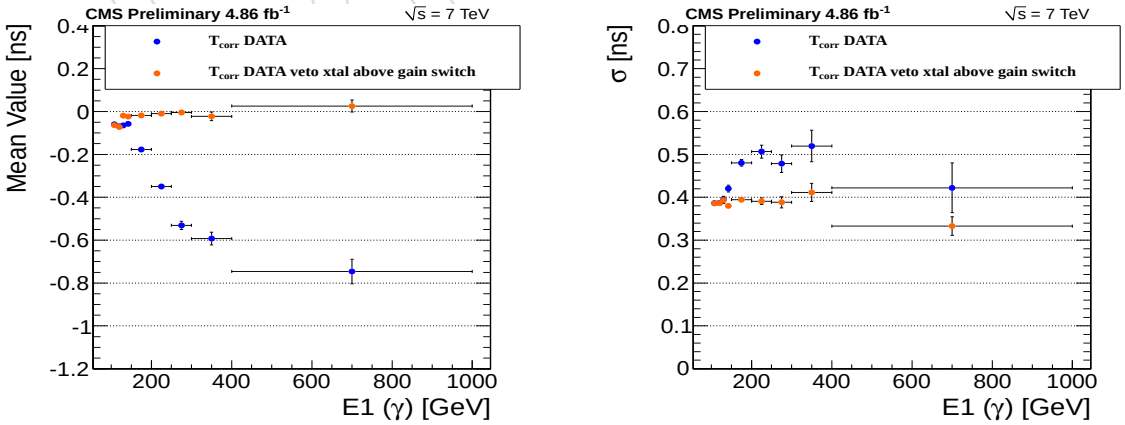

Figure 10: The energy dependance of the offset (left) and resolution (right) before and after mean time and gain switch corrections for data

4 Estimation of backgrounds

The importance of data-driven background determinations arises from the difficulty in modelling the tails of the QCD background, in predicting cross-sections for the SM backgrounds reliably, and predicting kinematic distributions such as the number of jets accurately. Therefore, we use data-driven techniques to estimate our main backgrounds, namely QCD and γ+jet. The remaining backgrounds present challenges but since they represent less than 0.6% of the total event sample we estimate their contribution using MC scaled to the luminosity of data.

4.1 Data-driven QCD

In order to select a reliable data sample of QCD we select events which pass the loose selection but fail the tight described in Table 2. This also includes a selection of 3 or more jets. We test our background estimation in Figure 11, where we require a good agreement between MC in the standard (blue) and MC in the control sample selections (red hatched), where the MC is normalised to the luminosity of data. In Figure 11 one can notice a deviation in data with respect to MC in the $\not\!\!E_{\mathrm{T}}$ estimate. The difference in the resolution for events with instrumental MET (multi-jet/gamma+jet) between data and MC is well known. And also something which worsens as a function of pile-up. For the ECAL timing, the overall poor modelling in MC is also well known. All in all, these are the motivating factors which lead us to using data-driven methods as much as possible in describing the shapes of our main backgrounds. Furthermore, the EWK contribution is estimated to be less than 1% in the QCD control sample selection (see Figure 24 right). and clean-up for PF Jets was studied as a possible source of discrepancy, however, Figure 23 shows that this is not the case. Furthermore, the signal contamination in both data control samples is less than 0.01%.

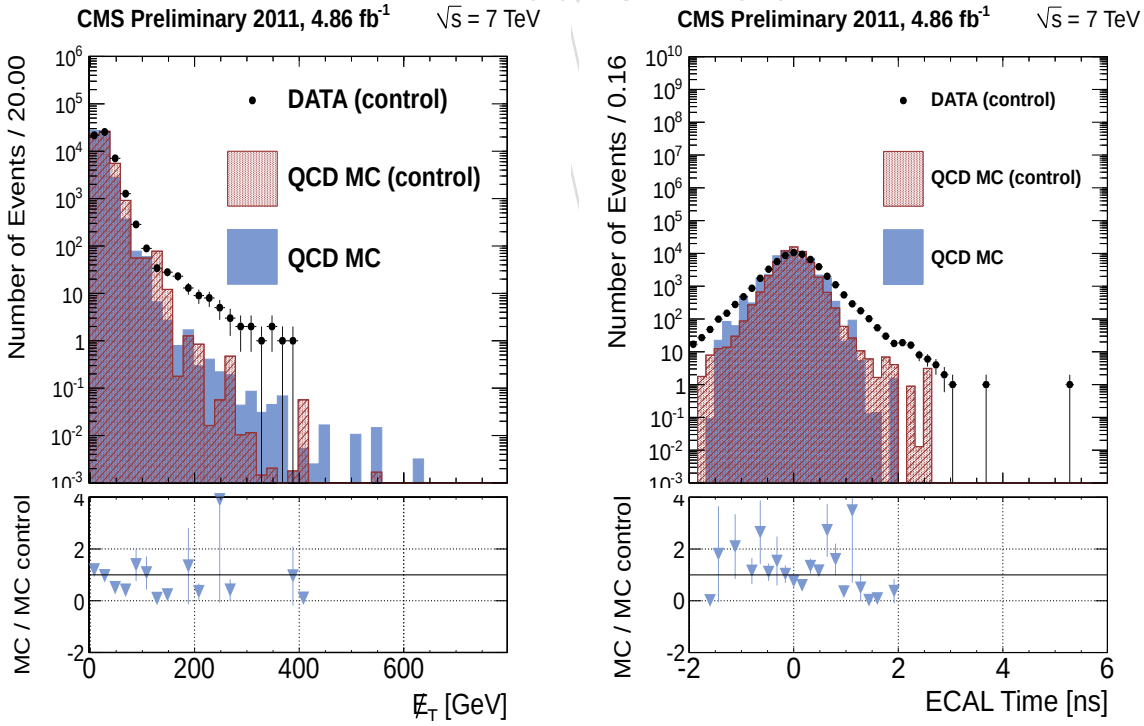

Figure 11: The distribution of the $\not\!\!E_{\mathrm{T}}$ (left) and timing (right) for the data-driven QCD estimate

4.2 Data-driven γ+jet

In order to select a reliable data sample of γ+jet we select events where:

- One photon passes the selection described in Table 2;
- The most energetic jet (jet1) is back to back with respect to the photon;
- $0.6 < p_T^{jet1}/p_T^{\gamma} < 1.4$;
- $0.2 > p_T^{jet2}/p_T^{\gamma}$.

We test our background estimation in Figure 12, where we require a good agreement between MC in the standard (brown) and MC in the control sample selections (red hatched), where the MC is normalised to the luminosity of data. We find that contribution of QCD in the γ+jet control sample is around 40% therefore we add a cut of $S_{Major} < 0.35$ optimized to reduce this contribution. After this cut the QCD contribution is reduced to 20%. Both QCD and γ+jet data control samples are statistically uncorrelated with data, and also much larger than the final signal sample. We estimate the uncertainty on our background determination by accounting for the statistical error, the error from the fitted number of background, and also the deviations between MC in the control sample and default selection. These correspond to the largest sources of uncertainty in the analysis, and will be discussed further in the Systematic Uncertainties section of this note.

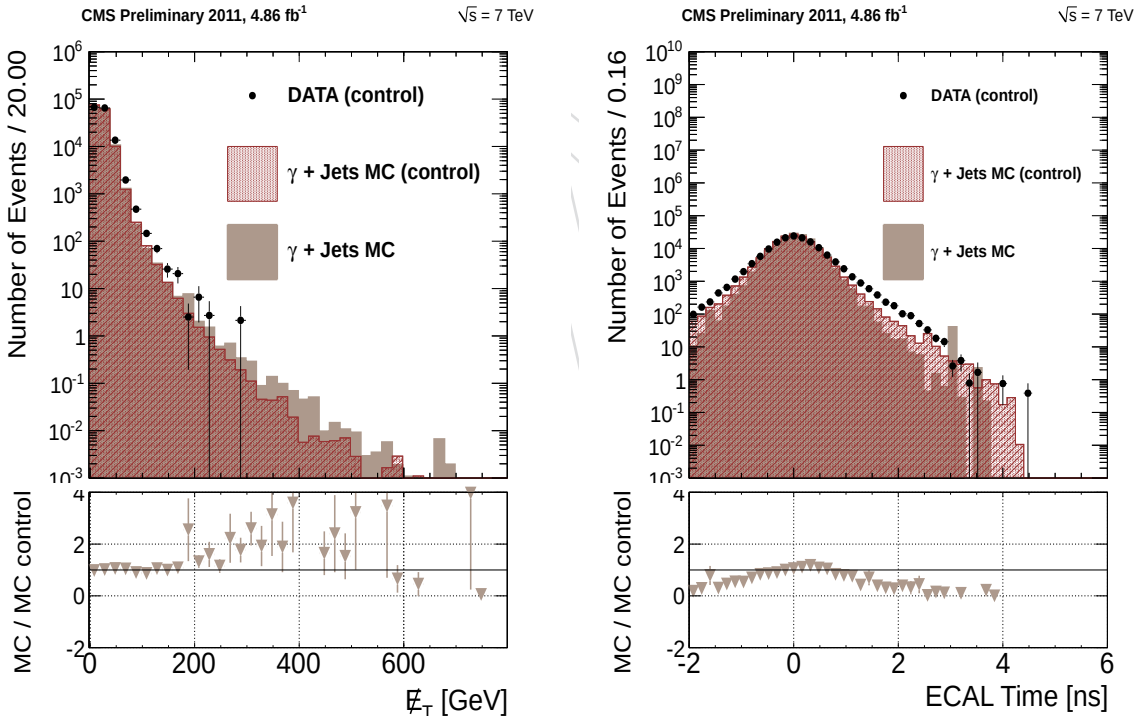

Figure 12: The distribution of the $\not{E}_T$ (left) and timing (right) of the data-driven γ+jet estimate

4.3 Re-weighting of ΣE_T

The control sample and default sample for γ+jet is expected to have have different ΣE_T distributions. This variable is the sum of the transverse energy of all the objects used to build the $\not{E}_T$. The difference is due to the difference in jet multiplicities between the standard selection and control sample selection. We improve this agreement by re-weighting the MC control sample

(red histograms in Figures 12) and data using the ΣE_T distributions. The $\not{E}_{\mathrm{T}}$ distribution before re-weighting is shown in Figure 24 (left) before and after re-weighting in Figure 12. The ΣE_T distribution can be seen before and after re-weighting in the appendix in Figure 25.

5 Systematic Uncertainties

There are several sources of systematic uncertainty which affect the analysis. The uncertainty on the luminosity $\mathcal{L}$ is taken using the current recommended value of 2.2%. This uncertainty for the jet energy scale correction has been estimated using the official CMSSW tool according to [22]. The uncertainty on the photon scale in the barrel was estimated to be 1.0% and based on the final-state radiation measurement with Z [23]. The uncertainties on the parton density functions (PDFs) are evaluated using the reweighting technique and Master Equation on the CTEQ65 model set as described in [24]. The uncertainty on the $\not{E}_{\mathrm{T}}$ resolution uses the conservative estimate of 10% respectively based on estimations from [25]. The uncertainty on the ECAL time is estimated this by calculating the discrepancy in the ECAL timing performance between γ+jet data and MC as a function of the photon energy. From these studies an uncertainty of 0.1 ns per event has been agreed by the ECAL DPG to be a conservative estimate. For the uncertainty on the background estimation we consider both the uncertainty due to statistics, and the uncertainty in the shape due to any discrepancies seen between the MC for the default selection and MC for the control sample selection. We account for the error given by the fit on the number of background events fitted ($\mathrm{Background}_{\mathrm{fit}}$), which will be described in Section 6.1. Also, we vary the background estimate bin-by-bin according to the poisson uncertainty due to statistics ($\mathrm{Background}_{\mathrm{stats}}$). For a further uncertainty on the derived shape of the data-driven backgrounds, we re-weight the $\not{E}_{\mathrm{T}}$ and timing according to differences seen in the shapes of the MC control sample and default selection ($\mathrm{Background}_{\mathrm{C.S.\ derivation}}$). We perform the re-weighting across the entire spectrum of $\not{E}_{\mathrm{T}}$ and ECAL timing in order to derive a conservative estimate as possible. We assess the total uncertainty on the fraction by which we fix the QCD and γ+jet ratio in the fit by taking the γ+jet contribution in MC and data (from our control sample), and calculating the difference in the total event yield (once scaled to luminosity) between the two. We expect the relavent uncertainties due to the Pythia cross-sections etc. to manifest themselves as this difference. This is calculated to be 8% ($\mathrm{Background}_{\mathrm{frac}}$). A summary of all the systematic uncertainties can be found listed in Table 3.

Source	Uncertainty (%)
Photon energy scale (1%)	$< 3.0\%$
Jet energy scale	$< 0.05\%$
Jet energy resolution (10%)	$< 1.9\%$
PDF uncertainties	$< 1.7\%$
$\not{E}_{\mathrm{T}}$ resolution (10%)	$< 1.5\%$
ECAL time uncertainty (0.1 ns)	$< 5.0\%$
$\mathrm{Background}_{\mathrm{stats}}$	$< 9.0\%$
$\mathrm{Background}_{\mathrm{C.S.\ derivation}}$	$< 5.4\%$
$\mathrm{Background}_{\mathrm{fit}}$	$< 0.3\%$
$\mathrm{Background}_{\mathrm{frac}}$ (8%)	$< 0.5\%$
Luminosity	2.2 %

Table 3: Summary of the systematic uncertainties on the signal (top) and background (middle)

6 Final distributions of $\not\!\!E_T$ and ECAL time

We see in Figure 13 the distribution $\not\!\!E_T$ and the ECAL time using data and MC after all analysis requirements. We see in Figure 14 the same distributions using the data-driven background estimates of QCD and γ+jet, where the background agreement to data has improved. Figure 15 shows the same criteria as Figure 14 with the criteria $\not\!\!E_T > 100$ for the ECAL time distribution (left), and ECAL time > 0.5 ns for the $\not\!\!E_T$ distribution (right). These plots are simply to illustrate the statistical power of the analysis in the background reduced regions of our analysis variables. Overall we see a very good agreement of data and our background estimate in Figure 14.

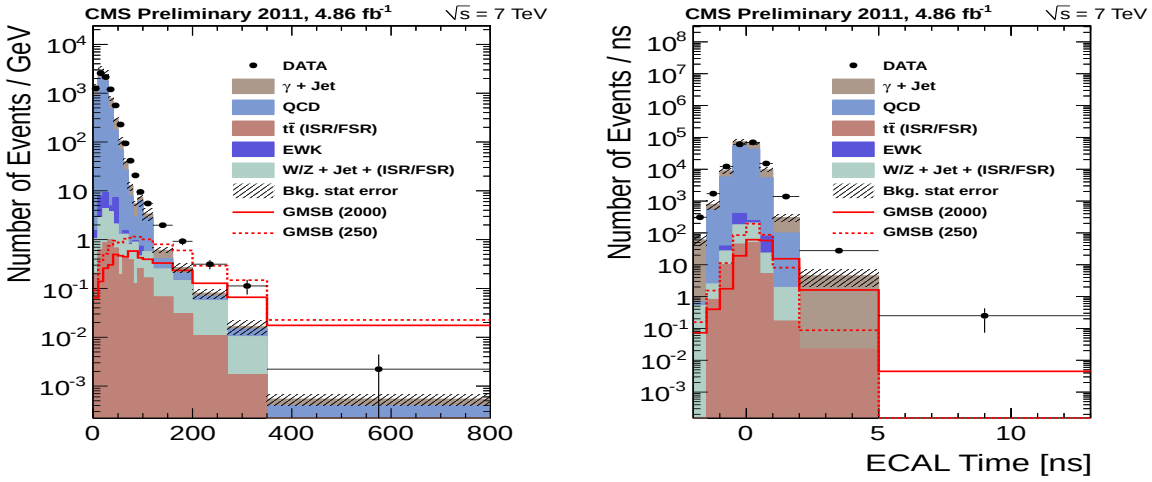

Figure 13: The distribution of the $\not\!\!E_T$ (right) and the ECAL time (left) with at least 3 jets above $P_T > 35$ for data and MC normalised to the luminosity of data after photon ID

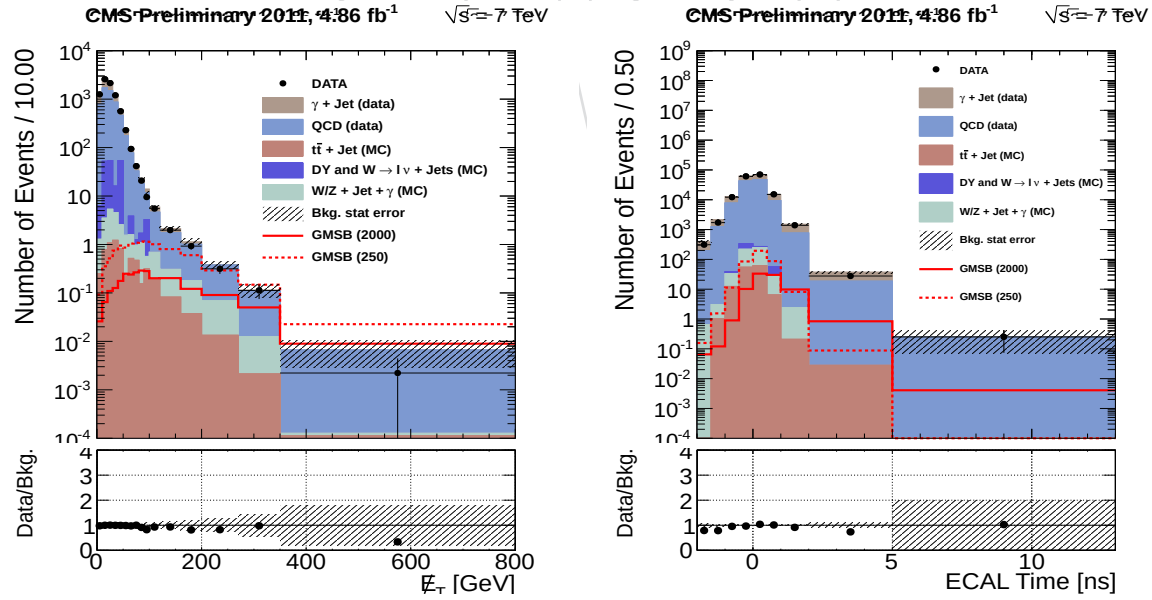

Figure 14: The distribution of the $\not\!\!E_T$ (right) and the ECAL time (left) with at least 3 jets above $P_T > 35$ using the data-driven background CSs described in Section 4, with background normalised to fitted values.

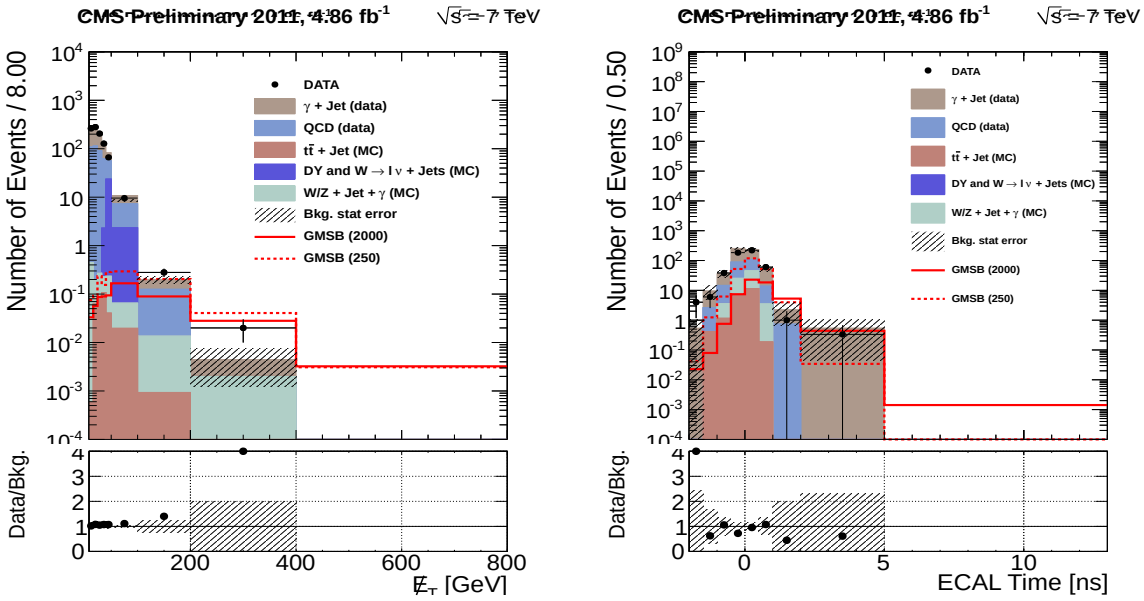

Figure 15: The distribution of the $\not\!\!E_{\mathrm{T}}$ with ECAL time $>$ 0.5 ns (right) and the ECAL time with $\not\!\!E_{\mathrm{T}} > 100\,\mathrm{GeV}$ (left) with at least 3 jets above $P_T > 35$ using data-driven background CS. The slight excess in data with respect to expected backgrounds is consistent with a no signal observation, and manifests itself with the observed limit being slightly higher than the expected.

6.1 Fit strategy

In order to estimate the total number of background and signal events in data we use a 2D maximum likelihood fit of signal and background to data, using the shapes of the $\not\!\!E_{\mathrm{T}}$ and ECAL timing distributions. For the QCD and γ+jet contribution we take the probability distribution function (PDF) from our data control samples. For $\mathrm{t\bar{t}}$ + jet, V+γ+jet, W+jets, and Drell Yan +jets we take the PDFs from MC and scale to the luminosity of data using the cross-sections provided by CMS. These MC events make up 0.6% of the total data sample but are accounted for since they could play a role in the tails of the $\not\!\!E_{\mathrm{T}}$ distribution where we would expect to find signal. The MC samples are thus fixed components in the fit. In order to improve the stability of the fit, we fix the normalisations of the QCD and γ+jet components relative to each other using fractions derived from MC (67% and 33% respectively). The uncertainty on our knowlegde of these two numbers is seen to be negligible for our final results. In summary, we use two floating components, signal and background (QCD and γ+jet). The result of the fit can be seen in Figure 16 with the number of events for each sample along with errors detailed in Table 4.

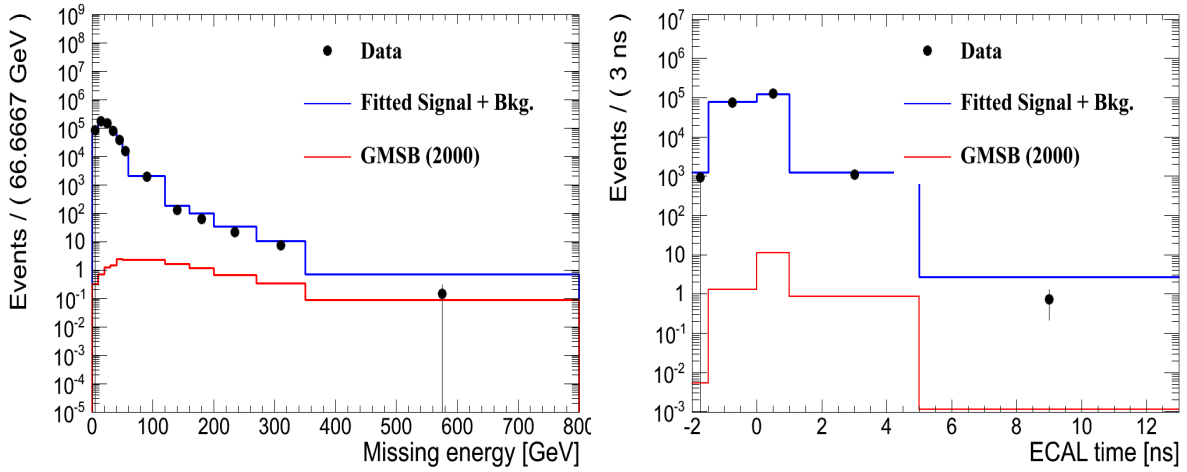

Figure 16: The distributions of $\not\!\!E_T$ (left) and ECAL timing (right) after the final fit for GMSB (250) signal and all backgrounds.

	No. Events
GMSB (250)	$6 \pm 8_{\text{fit}}$
GMSB (2000)	$4 \pm 4_{\text{fit}}$
QCD and γ+jet	$80916 \pm 285_{\text{fit}}$
$t\bar{t}$ + jet (fixed)	73
W + jets (fixed)	116
Drell-yan + jets (fixed)	67
W/Z + jets + ISR/FSR (fixed)	215
Data	81382

Table 4: The final number of events estimated for each component after all selection cuts and the final fit to data. The relative composition of QCD and γ+jet has been normalised to 67% and 33% with respect to each other and floated as one component.

6.2 Upper-limit calculation

The purpose of the fit is to estimate the amount of signal and background we observe. From Table 4 we do not see any excess beyond the expected SM events within statistical uncertainties, so therefore proceed to set upper-limits on the GMSB cross sections at 95% CL. The exclusion limits are calculated using the Asymptotic CLs [26] method with the user interface provided by the CMS Higgs group. We use the shape of 2D distributions for the MET and ECAL timing distributions in order to compute these limits and the results can be seen in Figure 17. We also cross-check our results using a Bayesian method which is compatible within one sigma (shown in Figure 26). Overall we see a good agreement of observed and expected limits, which is expected given the very good agreement seen in Figure 14. One can see for Figure 17 (left) that we are able to set a lower limit on the mass of the neutralino of around 220 GeV/c^2. From Figure 17 (right) we are also able to set a lower limit on the $c\tau$ of the neutralino of 6000 mm. Furthermore, we construct a 2D exclusion plot in the mass-lifetime plane of the $\tilde{\chi}_1^0$ which is shown in Figure 18.

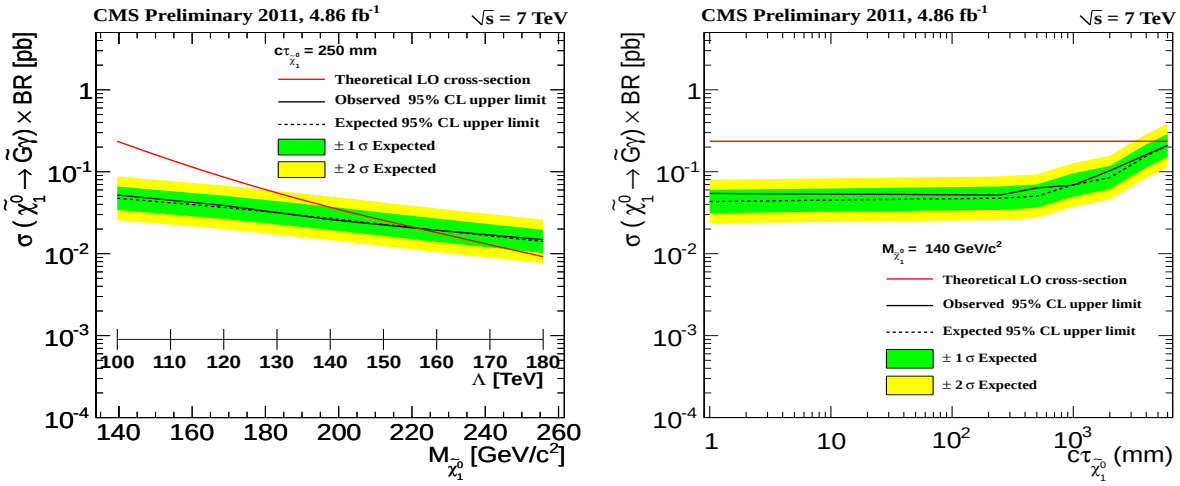

Figure 17: The observed 95% CL cross section upper limits as a function of the $\tilde{\chi}_1^0$ mass for $c\tau = 250$ mm (left), and the $\tilde{\chi}_1^0$ lifetime for $M_{\tilde{\chi}_1^0} = 140$ GeV (right) using Asymptotic CLs.

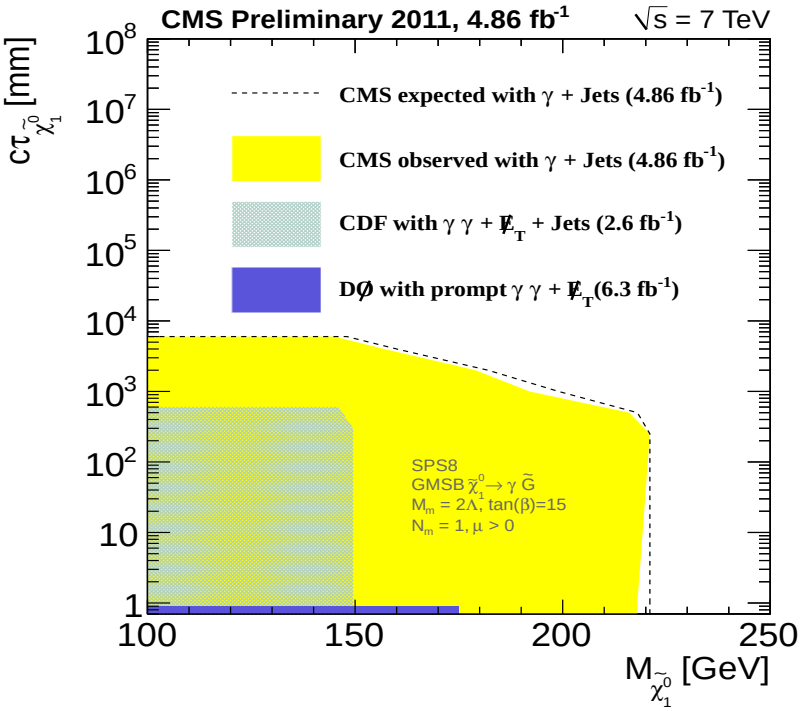

Figure 18: The observed exclusion region in the mass-lifetime plane of the $\tilde{\chi}_1^0$.

7 Conclusion

In conclusion, we have performed a search for displaced photons using 4.86 ± 0.11 fb^{-1} of CMS collision data at the centre-of-mass energy of 7 TeV. We use the Missing Transverse Energy and timing information from the ECAL to search for an excess of events over our SM background prediction. The data is found to be in good agreement with the expected contributions from Standard Model processes. We therefore proceed to set limits on the production cross-section of $\tilde{\chi}_1^0 \to \gamma\tilde{G}$ at 95% C.L. and place a lower limit of 220 GeV/c^2 and 6000 mm respectively on the mass and $c\tau_{\tilde{\chi}_1^0}$ of the $\tilde{\chi}_1^0$.

References

[1] G. F. Giudice and R. Rattazzi, "Theories with gauge-mediated supersymmetry breaking", *Phys. Rept.* **322** (1999) 419–499, doi:10.1016/S0370-1573(99)00042-3, arXiv:hep-ph/9801271.

[2] B. C. Allanach et al., "The Snowmass points and slopes: Benchmarks for SUSY searches", *Eur. Phys. J.* **C25** (2002) 113–123, doi:10.1007/s10052-002-0949-3, arXiv:hep-ph/0202233.

[3] D0 Collaboration Collaboration, "Search for diphoton events with large missing transverse energy in 6.3 fb^{-1} of $\mathbf{p\bar{p}}$ collisions at $\sqrt{\mathbf{s}} = \mathbf{1.96}$ TeV", *Phys.Rev.Lett.* **105** (2010) 221802, doi:10.1103/PhysRevLett.105.221802, arXiv:1008.2133.

[4] CDF Collaboration, "Search for Supersymmetry with Gauge-Mediated Breaking in Diphoton Events with Missing Transverse Energy at CDF II", *Phys. Rev. Lett.* **104** (2010) 011801, doi:10.1103/PhysRevLett.104.011801, arXiv:0910.3606.

[5] CMS Collaboration, "Search for new physics with long-lived particles decaying to photons and missing energy", *EXO-11-067* (2011).

[6] T. Sjostrand, S. Mrenna, and P. Z. Skands, "PYTHIA 6.4 Physics and Manual", *JHEP* **05** (2006) 026, doi:10.1088/1126-6708/2006/05/026, arXiv:hep-ph/0603175.

[7] J. Alwall, M. Herquet, F. Maltoni et al., "MadGraph 5 : Going Beyond", *JHEP* **1106** (2011) 128, doi:10.1007/JHEP06(2011)128, arXiv:1106.0522.

[8] GEANT4 Collaboration, "GEANT4: A simulation toolkit", *Nucl. Instrum. Meth.* **A506** (2003) 250–303, doi:10.1016/S0168-9002(03)01368-8.

[9] Z. Was, "TAUOLA the library for tau lepton decay, and KKMC/KORALB/KORALZ/... status report", *Nucl. Phys. Proc. Suppl.* **98** (2001) 96–102, doi:10.1016/S0920-5632(01)01200-2, arXiv:hep-ph/0011305.

[10] A. Djouadi, M. Muhlleitner, and M. Spira, "Decays of supersymmetric particles: The Program SUSY-HIT (SUspect-SdecaY-Hdecay-InTerface)", *Acta Phys.Polon.* **B38** (2007) 635–644, arXiv:hep-ph/0609292. 8 pages, no figures.

[11] CMS Collaboration, "Commissioning of the Particle-Flow Reconstruction in Minimum-Bias and Jet Events from pp Collisions at 7 TeV", *CMS PAS PFT-10-002* (2010).

[12] D. Franci, S. Rahatlou and D. del Re, "Studies for photons and neutral pions identication in the ECAL barrel region", *AN-08-075* (2008).

[13] https://twiki.cern.ch/twiki/bin/viewauth/CMS/PileupInformation.

[14] https://twiki.cern.ch/twiki/bin/view/CMS/PileupMCReweightingUtilities.

[15] CMS Collaboration, "Search for New Physics with a Mono-Jet and Missing Transverse Energy in pp Collisions at sqrt(s) = 7 TeV", *EXO-11-003* (2011).

[16] https://twiki.cern.ch/twiki/bin/view/CMS/HcalNoiseInfoLibrary.

[17] CMS Collaboration, "Beam Halo Event Identification in CMS Using the CSCs, ECAL, and HCAL", *AN-10-111* (2011).

[18] CMS Collaboration, "An algorithm for the determination of the flight path of long-lived particles decaying into photons", *EXO-11-212* (2010).

[19] CMS Collaboration, "The anti-kt jet clustering algorithm", *JHEP 0804* (2008) 6374, doi:10.1088/1126-6708/2008/04/063.

[20] CMS Collaboration, "Search for New Physics with Monojet Final States in pp collisions at sqrt(s) = TeV", *AN-11-228* (2011).

[21] CMS Collaboration, "Time Reconstruction and Performance of the CMS Electromagnetic Calorimeter", *JINST* **5** (2010) T03011, doi:10.1088/1748-0221/5/03/T03011, arXiv:0911.4044.

[22] CMS Collaboration, "Determination of the Jet Energy Scale in CMS with pp Collisions at sqrt(s) = 7 TeV", *JME-10-010* (2010).

[23] https://twiki.cern.ch/twiki/bin/viewauth/CMS/VGamma2011.

[24] A. Martin, W. Stirling, R. Thorne et al., "Parton distributions for the LHC", *Eur.Phys.J.* **C63** (2009) 189–285, doi:10.1140/epjc/s10052-009-1072-5, arXiv:0901.0002.

[25] CMS Collaboration, "Search for ADD Extra-dimensions with Photon + MET signature", *AN-11-319* (2011).

[26] G. Cowan, K. Cranmer, E. Gross et al., "Asymptotic formulae for likelihood-based tests of new physics", *Eur.Phys.J.* **C71** (2011) 1554, doi:10.1140/epjc/s10052-011-1554-0, arXiv:1007.1727.

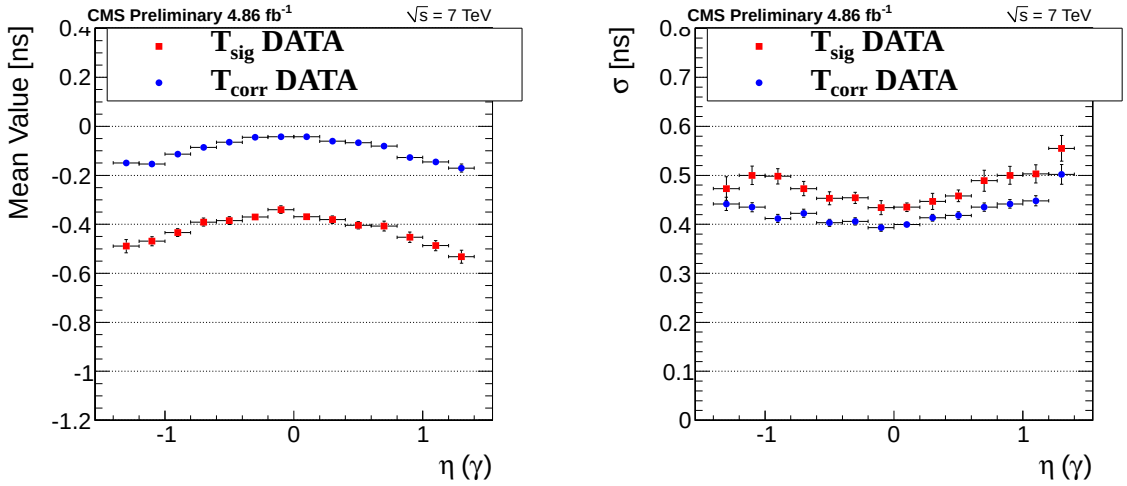

Figure 19: The η dependance of the offset (left) and resolution (right) before and after the mean time correction for data

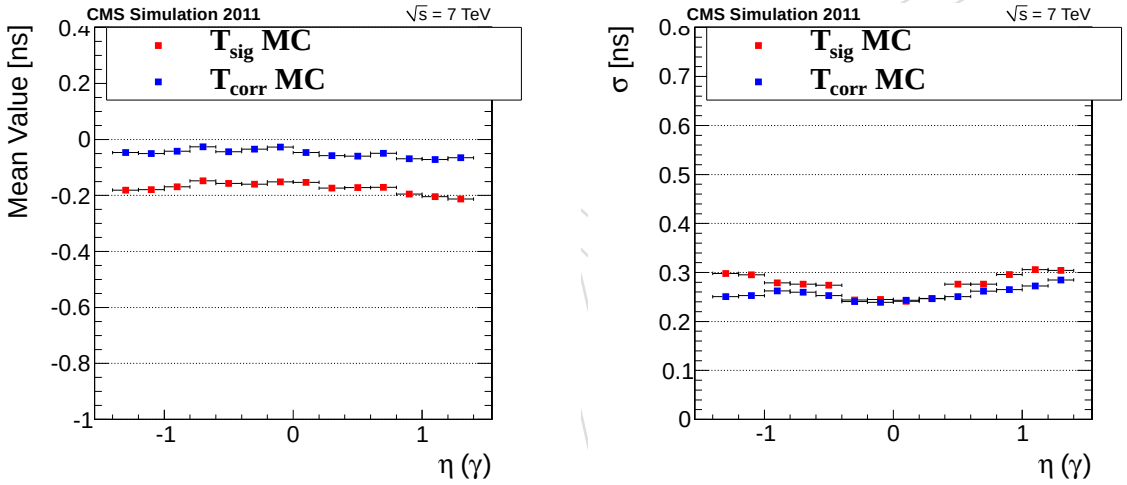

Figure 20: The η dependance of the offset (left) and resolution (right) before and after the mean time correction for MC

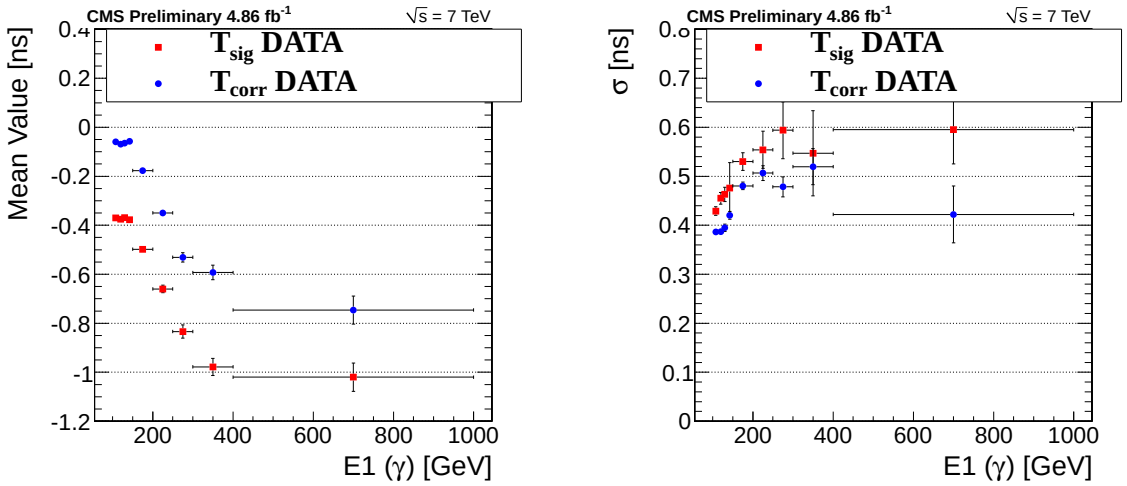

Figure 21: The energy dependance of the offset (left) and resolution (right) before and after the mean time correction for data

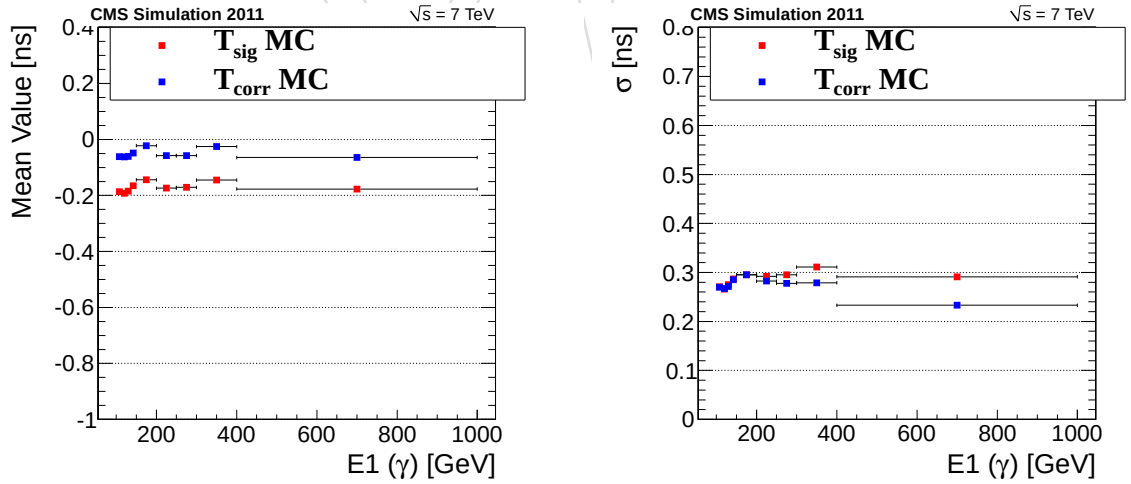

Figure 22: The energy dependance of the offset (left) and resolution (right) before and after the mean time correction for MC

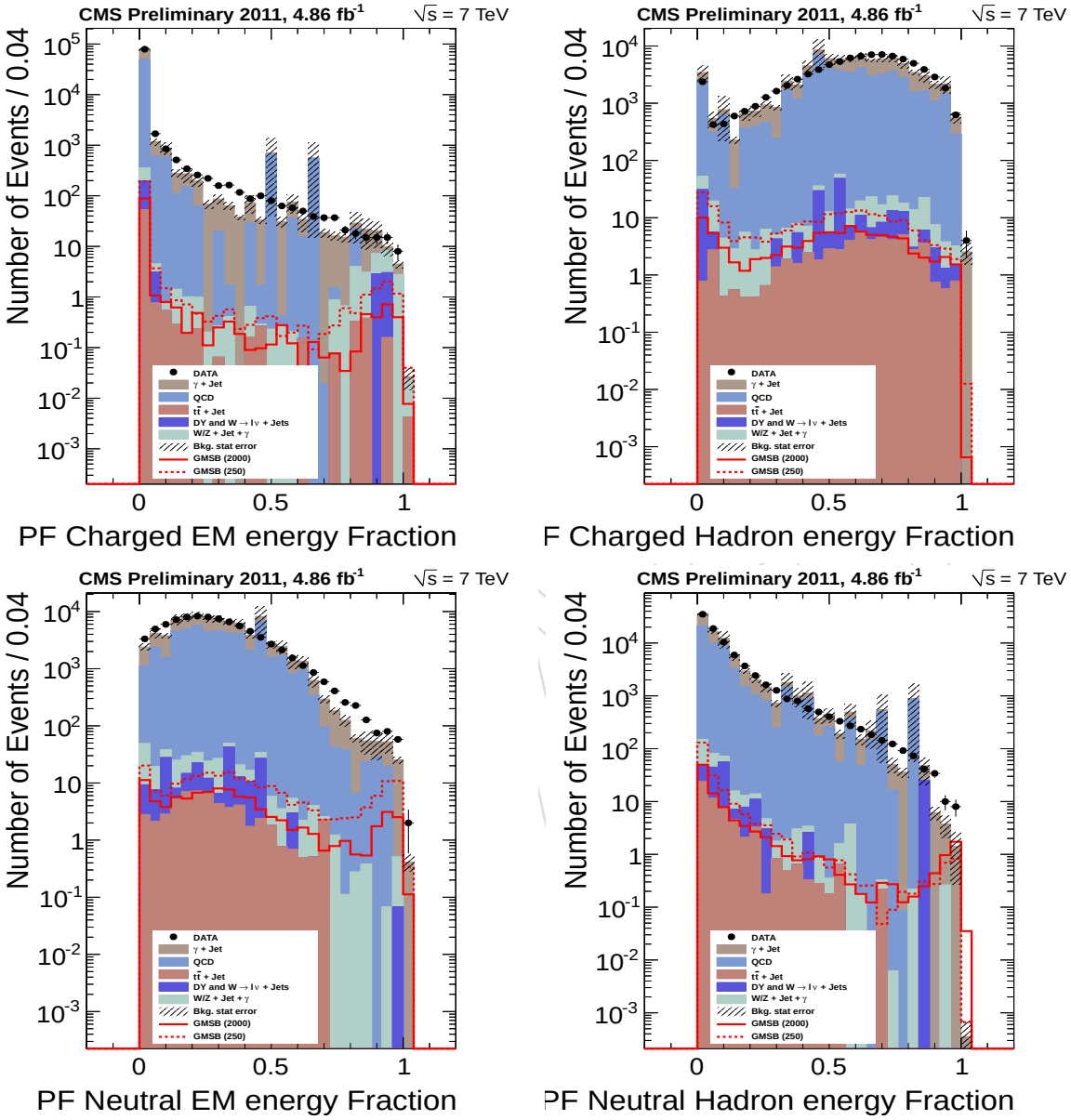

Figure 23: The distribution of the jet electromagnetic (top left) and hadronic (top right) energy fractions from charged and particles. The distributions of the jet electromagnetic (bottom left) and hadronic (bottom right) energy fractions from neutral particles.

Dataset name	σ_{LO} [pb]
GMSB_Lambda-100_CTau-1_7TeV_pythia6_cff/Summer11*	0.2357
GMSB_Lambda-100_CTau-250_7TeV_pythia6_cff/Summer11*	0.2357
GMSB_Lambda-100_CTau-500_7TeV_pythia6_cff/Summer11*	0.2357
GMSB_Lambda-100_CTau-1000_7TeV_pythia6_cff/Summer11*	0.2357
GMSB_Lambda-100_CTau-2000_7TeV_pythia6_cff/Summer11*	0.2357
GMSB_Lambda-100_CTau-3000_7TeV_pythia6_cff/Summer11*	0.2357
GMSB_Lambda-100_CTau-4000_7TeV_pythia6_cff/Summer11*	0.2357
GMSB_Lambda-100_CTau-6000_7TeV_pythia6_cff/Summer11*	0.2357
GMSB_Lambda-120_CTau-1_7TeV_pythia6_cff/Summer11*	0.0860
GMSB_Lambda-120_CTau-250_7TeV_pythia6_cff/Summer11*	0.0860
GMSB_Lambda-120_CTau-500_7TeV_pythia6_cff/Summer11*	0.0860
GMSB_Lambda-120_CTau-1000_7TeV_pythia6_cff/Summer11*	0.0860
GMSB_Lambda-120_CTau-2000_7TeV_pythia6_cff/Summer11*	0.0860
GMSB_Lambda-120_CTau-3000_7TeV_pythia6_cff/Summer11*	0.0860
GMSB_Lambda-120_CTau-4000_7TeV_pythia6_cff/Summer11*	0.0860
GMSB_Lambda-120_CTau-6000_7TeV_pythia6_cff/Summer11*	0.0860
GMSB_Lambda-140_CTau-1_7TeV_pythia6_cff/Summer11*	0.0368
GMSB_Lambda-140_CTau-250_7TeV_pythia6_cff/Summer11*	0.0368
GMSB_Lambda-140_CTau-500_7TeV_pythia6_cff/Summer11*	0.0368
GMSB_Lambda-140_CTau-1000_7TeV_pythia6_cff/Summer11*	0.0368
GMSB_Lambda-140_CTau-2000_7TeV_pythia6_cff/Summer11*	0.0368
GMSB_Lambda-140_CTau-3000_7TeV_pythia6_cff/Summer11*	0.0368
GMSB_Lambda-140_CTau-4000_7TeV_pythia6_cff/Summer11*	0.0368
GMSB_Lambda-140_CTau-6000_7TeV_pythia6_cff/Summer11*	0.0368
GMSB_Lambda-160_CTau-1_7TeV_pythia6_cff/Summer11*	0.0181
GMSB_Lambda-160_CTau-250_7TeV_pythia6_cff/Summer11*	0.0181
GMSB_Lambda-160_CTau-500_7TeV_pythia6_cff/Summer11*	0.0181
GMSB_Lambda-160_CTau-1000_7TeV_pythia6_cff/Summer11*	0.0181
GMSB_Lambda-160_CTau-2000_7TeV_pythia6_cff/Summer11*	0.0181
GMSB_Lambda-160_CTau-3000_7TeV_pythia6_cff/Summer11*	0.0181
GMSB_Lambda-160_CTau-4000_7TeV_pythia6_cff/Summer11*	0.0181
GMSB_Lambda-160_CTau-6000_7TeV_pythia6_cff/Summer11*	0.0181
GMSB_Lambda-180_CTau-1_7TeV_pythia6_cff/Summer11*	0.0092
GMSB_Lambda-180_CTau-250_7TeV_pythia6_cff/Summer11*	0.0092
GMSB_Lambda-180_CTau-500_7TeV_pythia6_cff/Summer11*	0.0092
GMSB_Lambda-180_CTau-1000_7TeV_pythia6_cff/Summer11*	0.0092
GMSB_Lambda-180_CTau-2000_7TeV_pythia6_cff/Summer11*	0.0092
GMSB_Lambda-180_CTau-3000_7TeV_pythia6_cff/Summer11*	0.0092
GMSB_Lambda-180_CTau-4000_7TeV_pythia6_cff/Summer11*	0.0092
GMSB_Lambda-180_CTau-6000_7TeV_pythia6_cff/Summer11*	0.0092

Table 5: Full description of the signal GMSB MC datasets used in this analysis

Λ (TeV)	100	120	140	160	180
$BF(\widetilde{G}+\gamma)$	94.0	90.4	87.7	84.6	83.0
$BF(\widetilde{G}+e^+e^-)$	2.0	1.9	1.9	1.8	1.8
$BF(\widetilde{G}+Z^0)$	3.6	7.7	11.0	13.5	15.3
$BF(\widetilde{G}+h^0/H_1^0)$	0.00001	0.00006	0.00010	0.00012	0.00013

Table 6: The description of the various branching fractions (%) for various processes in the signal MC

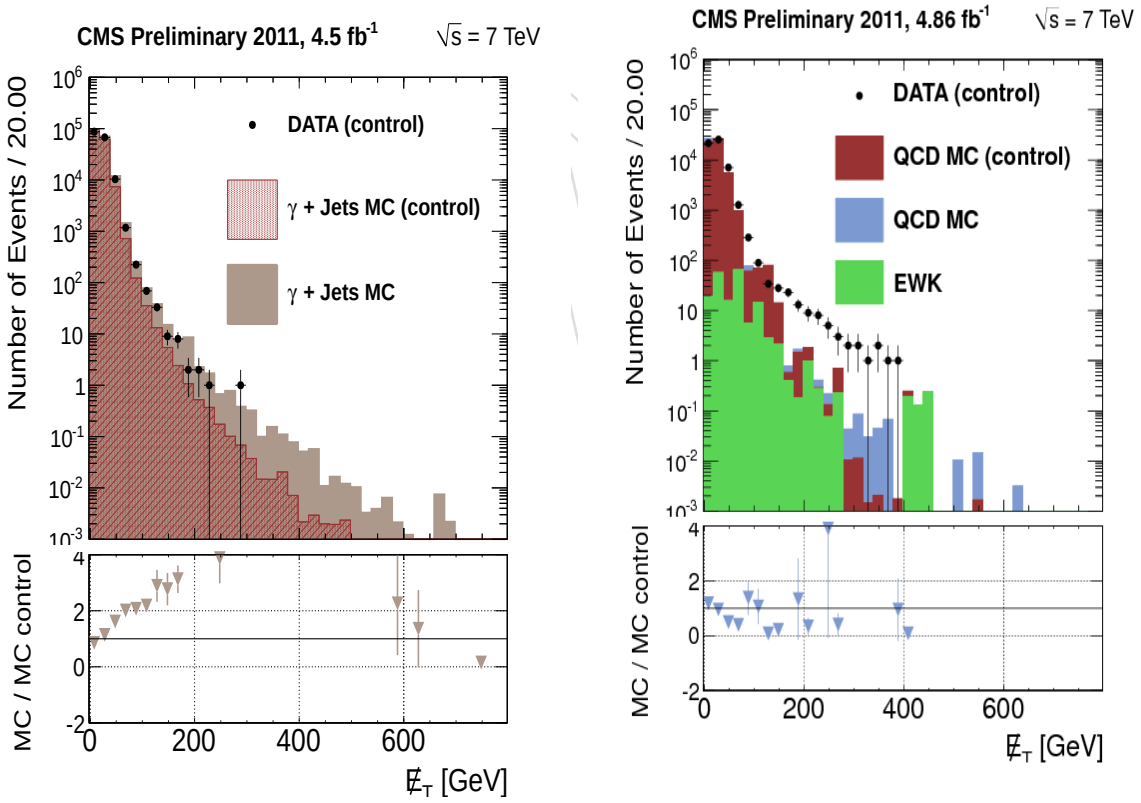

Figure 24: The distribution of the $\not\!\!E_T$ before ΣE_T re-weighting (left). The distribution of the $\not\!\!E_T$ for the QCD control sample with Drell-Yan, W + jets, $t\bar{t}$ + jets, W/Z + γ + jets (EWK) overlaid (right).

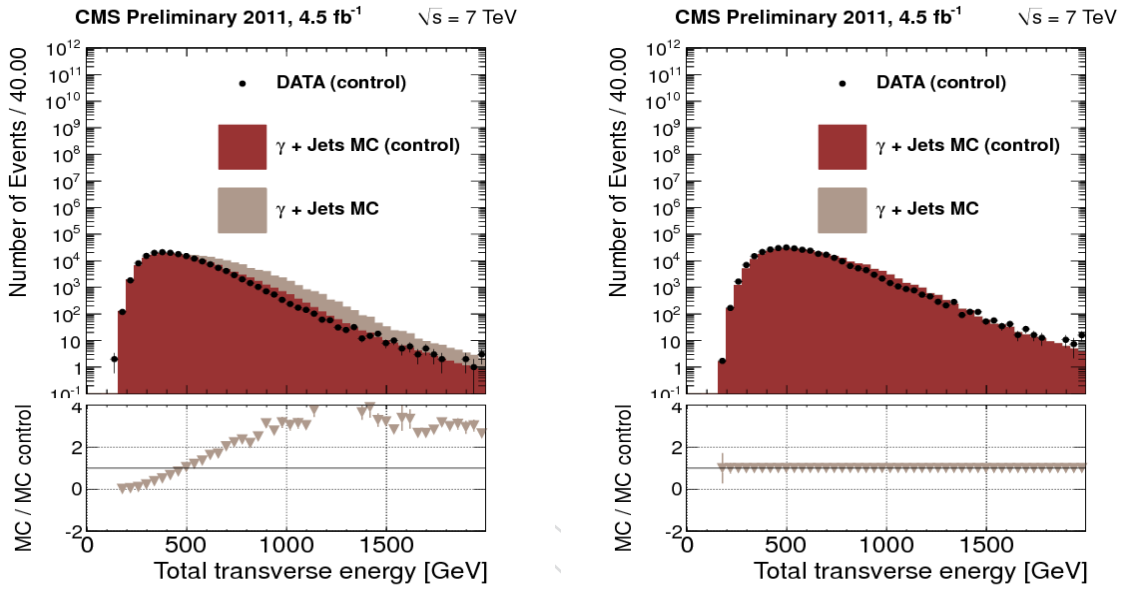

Figure 25: The distribution of the ΣE_T distribution before (left) and after (right) re-weighting.

Dataset name
G_Pt-*_TuneZ2_7TeV_pythia6-Summer11-PU_S3-AODSIM
QCD_Pt-*_TuneZ2_7TeV_pythia6-Summer11-PU_S3-AODSIM
WJetsToLNu_TuneZ2_7TeV-madgraph-tauola-Summer11-PU_S3-AODSIM
TTJets_TuneZ2_7TeV-madgraph-tauola-Summer11-PU_S4-AODSIM
DYJetsToLL_TuneZ2_M-50_7TeV-madgraph-tauola-Summer11-PU_S4-AODSIM
GVJets_7TeV-madgraph-Summer11-PU_S4-AODSIM

Table 7: The description of the background MC samples used in this analysis

%	GMSB $c\tau = 250$ $\Lambda = 100$	GMSB $c\tau = 2000$ $\Lambda = 100$	GMSB $c\tau = 4000$ $\Lambda = 100$	GMSB $c\tau = 250$ $\Lambda = 140$	GMSB $c\tau = 250$ $\Lambda = 180$
Pre-selection	61	37	25	76	82
$P_T(\gamma)$	63	54	52	77	86
$N_{jets} \geq 3$	66	60	58	71	77
Halo Veto	100	100	100	100	100
$\|\eta\|$	93	94	94	92	94
Electrons	91	87	77	93	93
S_{Minor}	99	99	99	99	99
HCAL Iso	99	99	99	99	99
ECAL Iso	92	90	88	95	96
Track Iso	96	97	96	96	96
ECAL time	100	100	100	100	100
Not γ+jet	99	99	99	99	99
Topological	91	94	95	90	88
ϵ_{TOT}	18.4	8.4	4.6	29	38

Table 8: The efficiencies for the selection criteria on signal MC.

%	γ+jet	QCD	$t\bar{t}$ + jet	V+γ+jet	W+jets	Drell Yan +jets	Data
Pre-selection	50	0.35	4	3	0.3	0.9	6.5
$P_T(\gamma)$	25	14	37	35	24	24	43
$N_{jets} \geq 3$	6	11	81	24	17	30	11
Halo Veto	100	100	100	100	100	100	99
$\|\eta\|$	72	86	92	84	77	80	82
Electrons	98	55	4	62	3	2	77
S_{Minor}	99	67	80	98	79	90	89
HCAL Iso	99	99	98	99	100	98	99
ECAL Iso	98	69	64	95	64	72	94
Track Iso	95	87	67	92	100	81	93
ECAL time	100	100	100	100	100	100	99
Not γ+jet	98	99	100	99	100	99	98
Topological	91	95	97	94	100	100	93
ϵ_{TOT}	4.5×10^{-1}	1.1×10^{-3}	1.5×10^{-4}	9.9×10^{-4}	8.8×1.4^{-6}	6.6×10^{-6}	8.8×10^{-2}

Table 9: The efficiencies for the selection criteria on data and background MC.

%	$c\tau = 1$ mm	$c\tau = 250$ mm	$c\tau = 500$ mm	$c\tau = 1000$ mm	$c\tau = 2000$ mm	$c\tau = 4000$ mm	$c\tau = 6000$ mm
$\Lambda = 100$ TeV	18.7 $\pm$0.3	18.4 $\pm$0.2	16.9 $\pm$0.2	12.7 $\pm$0.2	8.4 $\pm$0.2	4.6 $\pm$0.1	3.3 $\pm$0.1
$\Lambda = 120$ TeV	24.9 $\pm$0.4	24.6 $\pm$0.3	23.2 $\pm$0.3	20.2 $\pm$0.3	15.1 $\pm$0.4	9.4 $\pm$0.1	6.6 $\pm$0.1
$\Lambda = 140$ TeV	30.4 $\pm$0.3	31.3 $\pm$0.3	30.9 $\pm$0.5	28.1 $\pm$0.5	22.2 $\pm$0.4	15.6 $\pm$0.2	11.4 $\pm$0.3
$\Lambda = 160$ TeV	35.5 $\pm$0.3	36.1 $\pm$0.6	36.8 $\pm$0.5	34.5 $\pm$0.6	29.4 $\pm$0.4	21.2 $\pm$0.3	17 $\pm$0.4
$\Lambda = 180$ TeV	40.1 $\pm$0.7	38.0 $\pm$0.5	40.8 $\pm$0.6	40.1 $\pm$0.6	36.0 $\pm$0.5	28.1 $\pm$0.3	22.2 $\pm$0.4

Table 10: The selection efficiencies for all the signal samples used in this analysis. The errors quoted are from the systematics.

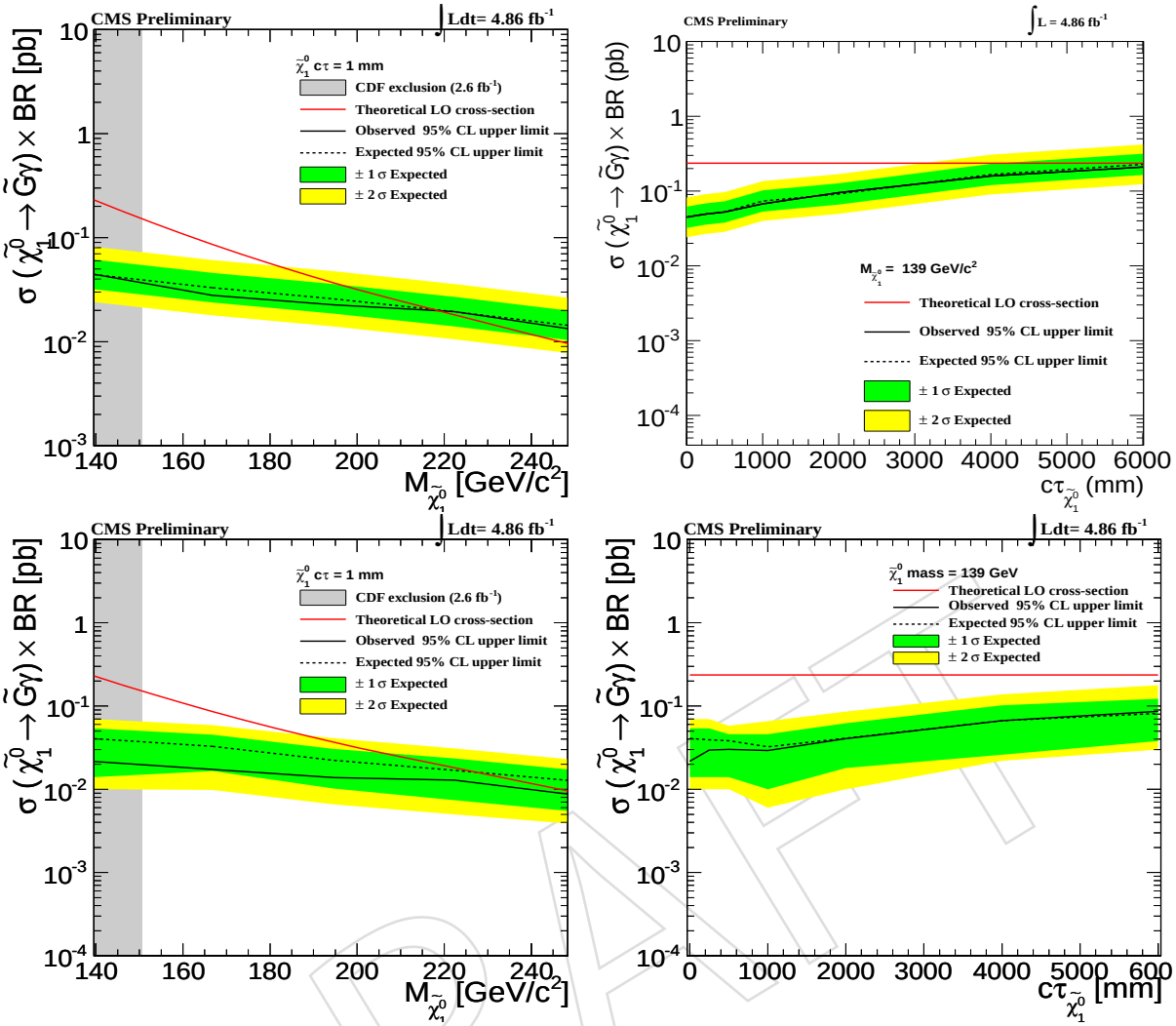

Figure 26: A comparison of the observed 95% CL cross section upper limits as a function of the $\tilde{\chi}_1^0$ mass for $c\tau = 1$ mm (left), and the $\tilde{\chi}_1^0$ lifetime for $M_{\tilde{\chi}_1^0} = 139$ GeV (right) using CLs (top) and our Bayesian method (bottom).

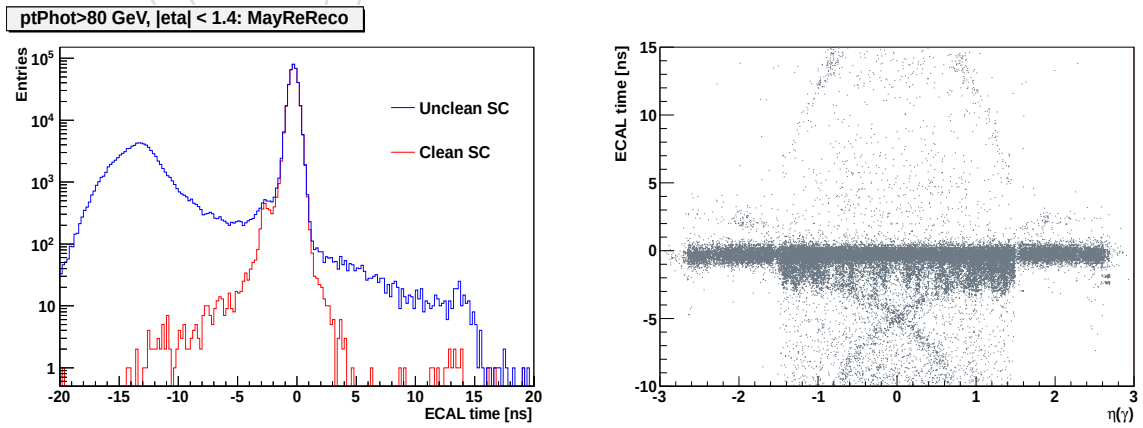

Figure 27: The ECAL time distribution of cleaned and uncleaned photons overlaid for data (right) and the ECAL time vs $\eta(\gamma)$ distribution (left)

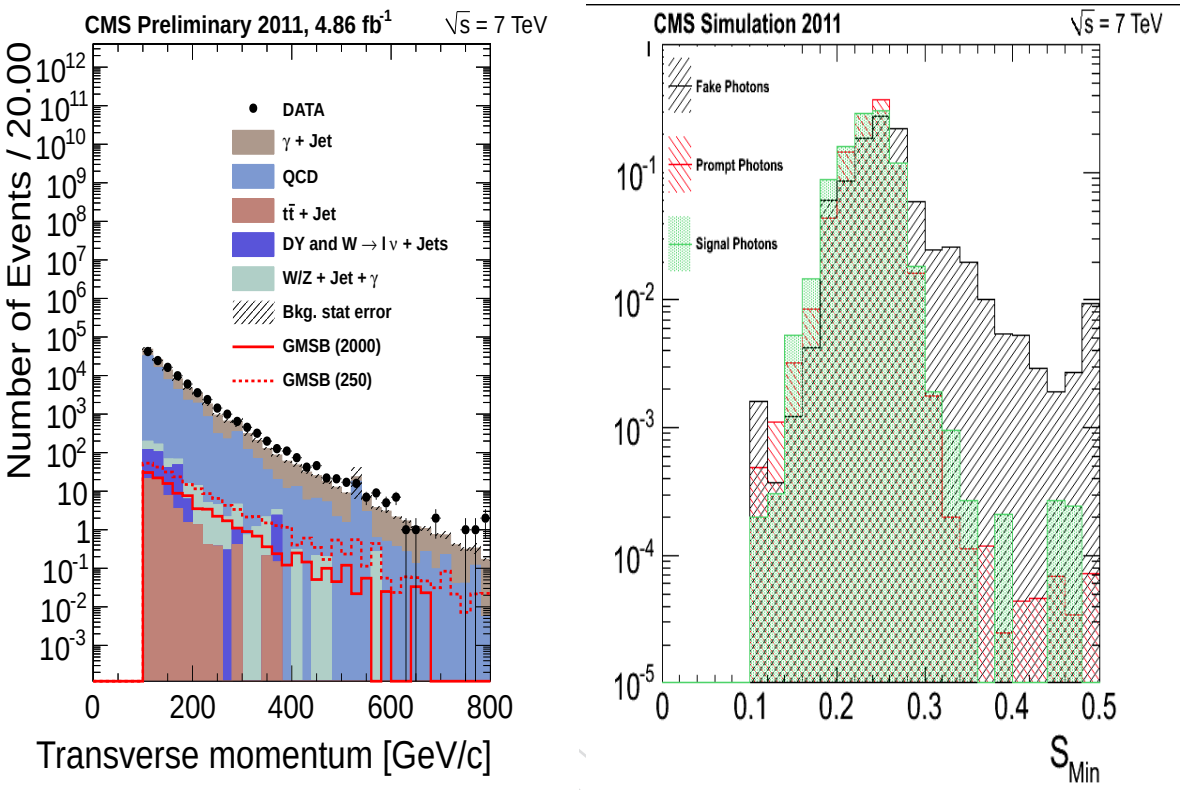

Figure 28: The distribution of the number of the photon P_T with at least 3 jets above $P_T > 35$ for data and MC normalized to the luminosity of data after photon ID (left). The distribution of the number of S_{Minor} for prompt and fake photons scaled to area (right).

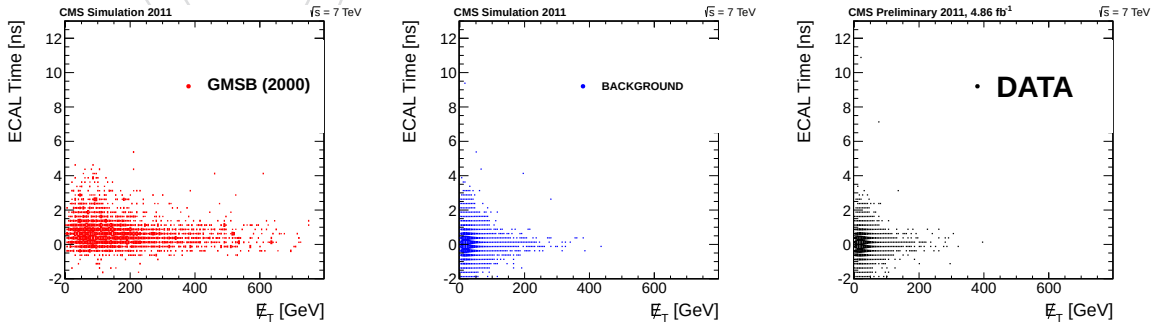

Figure 29: The 2D distribution of $\not{E}_T$ and ECAL time for signal (left), all background (middle), data (right).

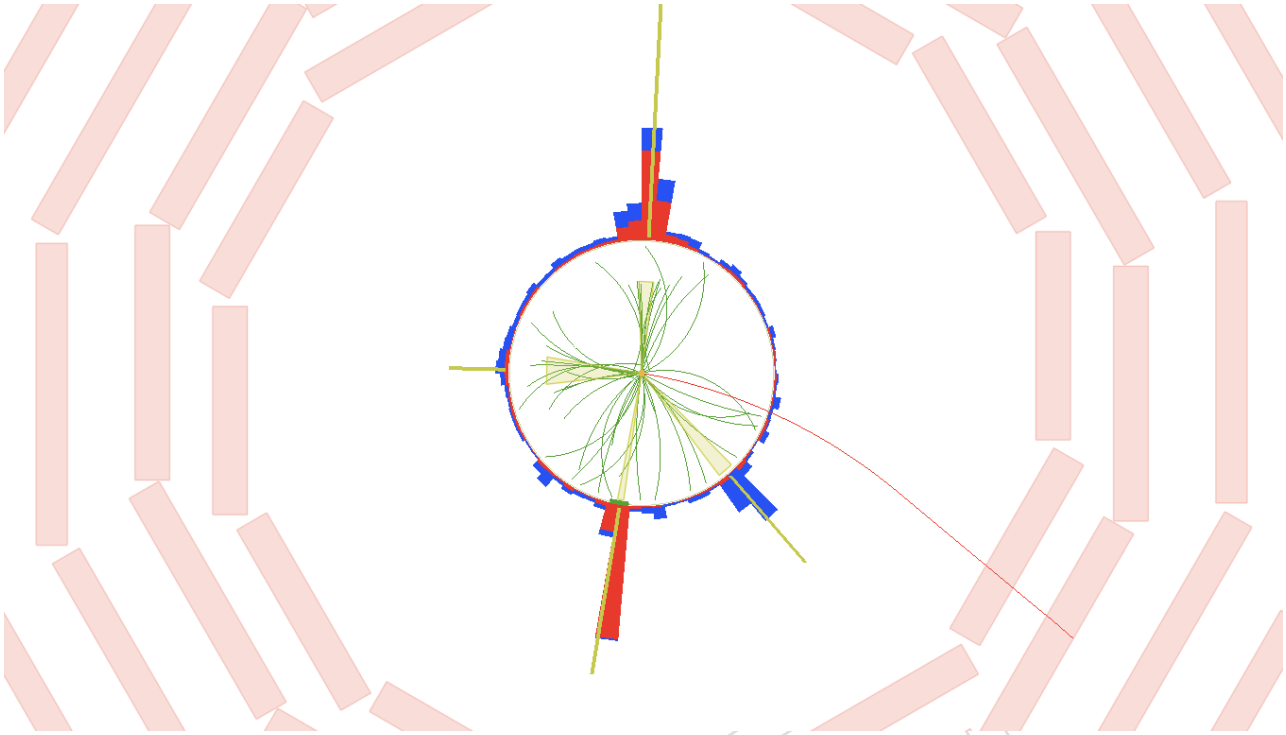

Figure 30: A $\rho - Z$ view of the highest ECAL time event in the signal data sample, where the ECAL time = 10.7 ns, P_T=120 GeV/c, and $\not{E}_T$ = 18 GeV

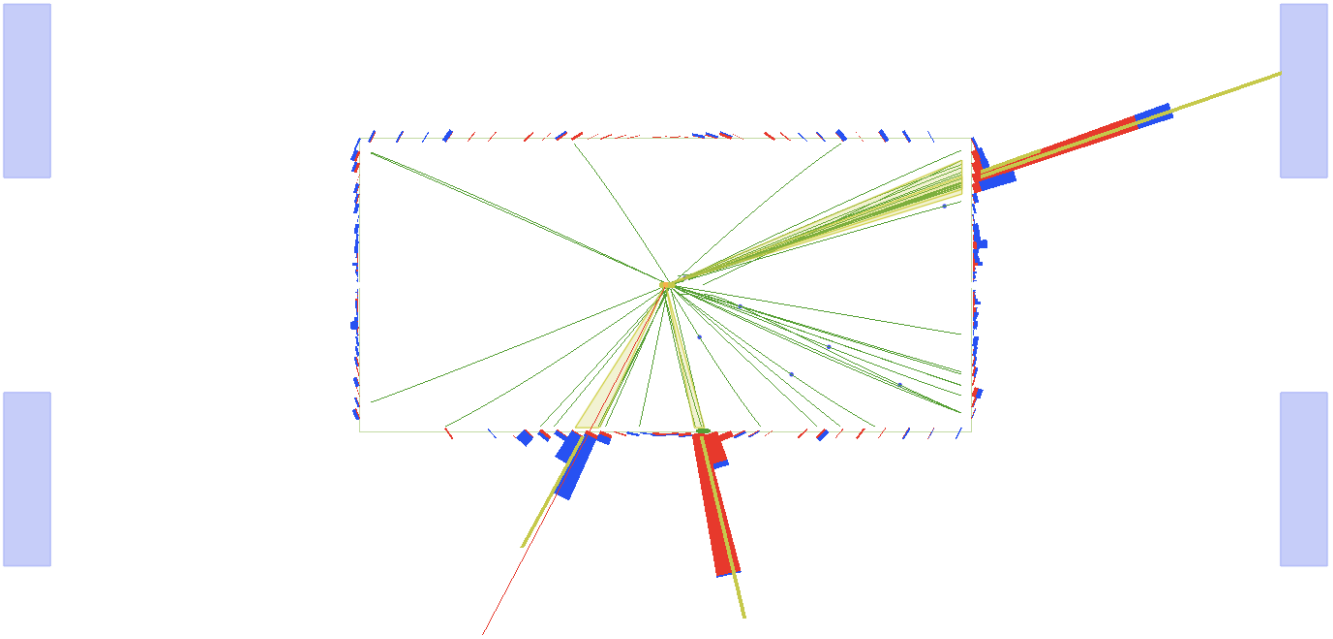

Figure 31: A $\rho - \phi$ view of the highest ECAL time event in the signal data sample, where the ECAL time = 10.7 ns, P_T=120 GeV/c, and $\not{E}_T$ = 18 GeV

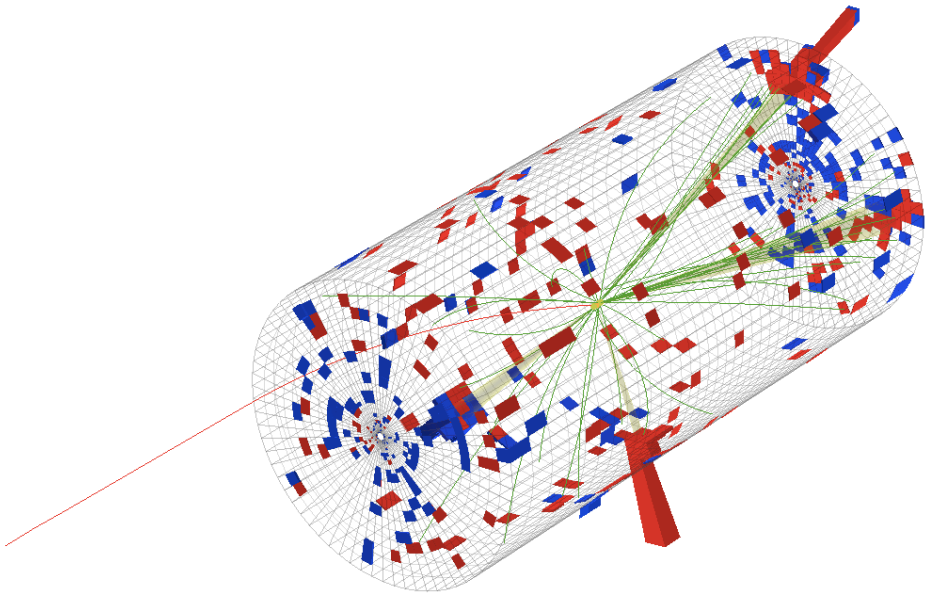

Figure 32: A 3D view of the highest ECAL time event in the signal data sample, where the ECAL time = 10.7 ns, P_T=120 GeV/c, and $\not{E}_T$ = 18 GeV